國立臺灣大學理學院物理學研究所

博士論文

Graduate Institute of Physics

College of Science

National Taiwan University

Doctoral Dissertation

二維材料結構中高度純淨界面的自旋傳輸現象

Spin-transport Phenomena in 2D Materials-Based Structures with Ultraclean Interfaces

黃鼎鈞

Ting-Chun Huang

指導教授: 謝馬利歐 博士

Advisor: Mario Hofmann Ph.D.

中華民國 112 年 12 月

December, 2023

doi:10.6342/NTU202400068

Acknowledgements

A wonderful journey is made more enjoyable with good companionship, turning long and distant travels into relaxed and pleasant experiences. Many people can reach the summit of a mountain, yet the experiences along the way vary greatly. Obtaining a doctoral degree is not uncommon, but the feelings and insights gained from the journey differ. I am grateful for the companions prepared for me by our Heavenly Father on this journey.

My closest companion is my advisor, Mario Hofmann. Thank you for granting students the utmost trust and significant freedom, enabling me to learn to creatively solve problems rather than laboring solely for achievements. This has gradually built my independent research skills in identifying and simplifying problems, exploring physics, seeking solutions, and improving applications. Moreover, you are an example of a work-life balance, teaching me how to be a good father and husband, helping me achieve balance in work, family, and life. Mario Hofmann's friendly interactions and mutual respect have influenced me beyond the enhancement of scientific expertise. I also appreciate Professor Ya-Ping Hsieh for her concern and arrangements regarding my career planning and life needs. Learning within the research group you both co-lead brings me a great satisfaction.

I want to thank my parents for providing me with the opportunity to study without worries and for their full support on this journey. To my elder brothers in my family, thank

doi:10.6342/NTU202400068

you for being role models of diligence and upward striving. I am grateful to the pastors and brothers and sisters in the fellowship who often encourage and pray for me. Special thanks to my friends in the laboratory for creating a joyful atmosphere during our work process.

I want to express special gratitude to my wife, Chia-Hua Lin. Thank you for supporting me in completing my doctoral degree and building our family together. Journeying through life with you is the greatest happiness. To my son, Miles Huang, writing my thesis while holding you in the cold winter is truly warm. Although you often delete my sentences, it happens to help me refine the content.

Finally, I want to thank our Heavenly Father for allowing me to know more of Your glory and abundant provisions beyond what I sought or imagined during the pursuit of my doctoral journey.

Psa 139:14 I will give you praise, for I am strangely and delicately formed; your works are great wonders, and of this my soul is fully conscious.

一趟美好的旅行，是因為有良伴同行，遠途又漫長旅程，也因此變得輕鬆愜意。很多人一樣能登山攻頂，路上所經歷的確截然不同，取得博士學位的人不在少數，其中所經驗的也大不相同，我感謝這趟旅程中，天父為我所預備的良伴。

最密切的良伴就是我的指導教授 Mario Hofmann。謝謝你給予了學生最大的信任及高度的自由，使我能夠學習以創意解決問題，而非以苦力拚業績，以至於逐漸地建立起發現問題、簡化問題、探索物理、尋找解方及改善應用的獨立研究能力。不僅如此，你是一位工作生活平衡的模範，在你身上我學習如何成為一位好父親、好丈夫，幫助我能在工作、家庭、生活中均衡的發展。Mario Hofmann 與人的友善互動及相互尊重對我的影響超越了科學研究的提升。同時，我也感謝

doi:10.6342/NTU202400068

謝雅萍教授對於我在職涯規劃及生活需要上的關心與安排，在你們夫婦共同主持的研究團隊中學習，我感到非常幸福與滿足。

我要感謝我的父母，使我能無後顧之憂地學習，並且在這趟旅途中全力的支持，還有家中的兄長們，成為我努力向上的榜樣。我也要感謝團契中的牧長及弟兄姊妹，時常給我鼓勵，為我禱告。我也感謝實驗室的好朋友，一起建立愉快的氛圍，因此，工作過程中總是充滿歡笑。

我要特別感謝我的妻子林佳樺，謝謝妳支持我完成博士學位，並且一起建造家庭，能與妳同行在人生的旅途，是最幸福的事情。還有我的兒子 Miles Huang，在寒冷的冬天中寫論文，還能同時把你抱在身上真的好溫暖，也因為你常常把我打的字刪掉，所以我可以把每一個文句修得更好。

最後，我要謝謝天父，讓我在攻讀博士的旅途中，更多認識祢的榮耀及祢的豐富預備，都超過我所求所想。

詩篇 139:14 我要稱謝你，因我受造奇妙可畏，你的作為奇妙，這是我心深知道的。

doi:10.6342/NTU202400068

doi:10.6342/NTU202400068

摘要

二維材料與磁性自旋閥的整合被期望能夠開啟自旋電子學裝置的潛力。然而，目前的實際情況仍然偏離預期。大多數研究將這樣的差距歸因於在二維材料與其鐵磁性電極界面之間的汙染。我們研發了能製作超高潔淨界面的製程方法。通過在真空環境中一次性且同步地沉積非對稱鐵磁電極在懸浮的二維材料上，可以有效地避免氧化和界面汙染的負面效應。在我們的研究中，基於石墨烯的自旋閥在界面與鐵磁材料呈現強烈的相互作用，產生比起以往的實驗結果更高的磁阻值。不僅如此，鐵磁性電極可以展現固有的矯頑力，而不受污染物干擾，這使我們能夠藉由額外的反鐵磁材料來製造具有可控矯頑力的自旋閥。此外，基於二硫化鉬的自旋閥的金屬鄰近效應和主導的自旋過濾效應，呈現出顯著的負磁阻值。這些發現不僅增強了自旋電子學在實際應用中的可行性，還探索了可延伸更多功能性的自旋閥機制。我們的方法提供了一條有效探討鐵磁性電極與二維材料之間固有相互作用的反應途徑。

關鍵字：自旋電子學、自旋閥、二維材料、石墨稀、磁阻、純淨界面

doi:10.6342/NTU202400068

doi:10.6342/NTU202400068

Abstract

The integration of 2D materials and magnetic spin valves is expected to unlock the potential of spintronics devices. However, the current practical situation still deviates from expectations. Most studies attribute such inconsistencies to the challenge of achieving a contamination-free interface between the 2D material barrier and its ferromagnetic contacts. Here, we demonstrate a novel approach to ensure an ultrahigh clean interface. By synchronously depositing asymmetric contacts on a suspended 2D material in a single step within a vacuum environment, the detrimental effects of oxidation and breaks in the interface can be effectively avoided. In our study, graphene-based spin valves present a strong interaction at the interface that gives rise to exceptional magnetoresistance values. Ferromagnetic electrodes can exhibit inherent coercivity without pollutant disturbance, allowing us to manufacture a spin valve with controllable coercivity by incorporating additional antiferromagnetic materials. Moreover, MoS_2-based spin valves exhibit remarkable negative magnetoresistance values due to the metallic proximity effect and the predominant

doi:10.6342/NTU202400068

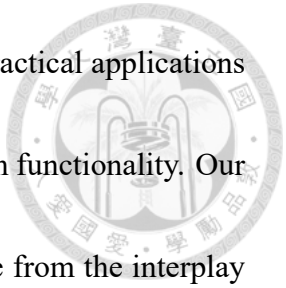

spin filter effect. These findings not only enhance the feasibility of practical applications in spintronics but also explore the mechanisms of spin valves with rich functionality. Our method evidently provides a path to investigate the intrinsic response from the interplay between ferromagnetic electrodes and 2D materials.

Keywords: Spintronics, Spin valve, 2D materials, Graphene, Magnetoresistance, Ultra-clean interface

doi:10.6342/NTU202400068

Contents

doi:10.6342/NTU202400068

doi:10.6342/NTU202400068

doi:10.6342/NTU202400068

doi:10.6342/NTU202400068

List of Figures

doi:10.6342/NTU202400068

doi:10.6342/NTU202400068

doi:10.6342/NTU202400068

doi:10.6342/NTU202400068

List of Tables

doi:10.6342/NTU202400068

doi:10.6342/NTU202400068

Chapter 1 Introduction

1.1 Spin valve

Spintronics, an evolving field harnessing the intrinsic spin of electrons alongside their fundamental electronic charge for information processing and storage, shows great potential in overcoming the limitations of traditional charge-based electronic devices, offering advantages such as faster operation, higher efficiency, and a more compact arrangement.[1–3]

Spin is intricately connected with phenomena encompassing band splitting, polarized light, thermal gradients, external electric fields, and magnetic forces. As illustrated in the Figure 1.1, the application of spin extends broadly across various technological domains. Thus, a profound comprehension of the underlying mechanisms governing spin interactions among materials holds the promise of technological breakthroughs. Our primary focus is on spin injection from the ferromagnet.

The spin valve is a critical building block at the heart of spintronic devices. Its structure includes two ferromagnetic electrodes flanking a spacer in the middle. This sandwich-like architecture facilitates the transition between parallel and antiparallel spins through the application of an external magnetic field.

doi:10.6342/NTU202400068

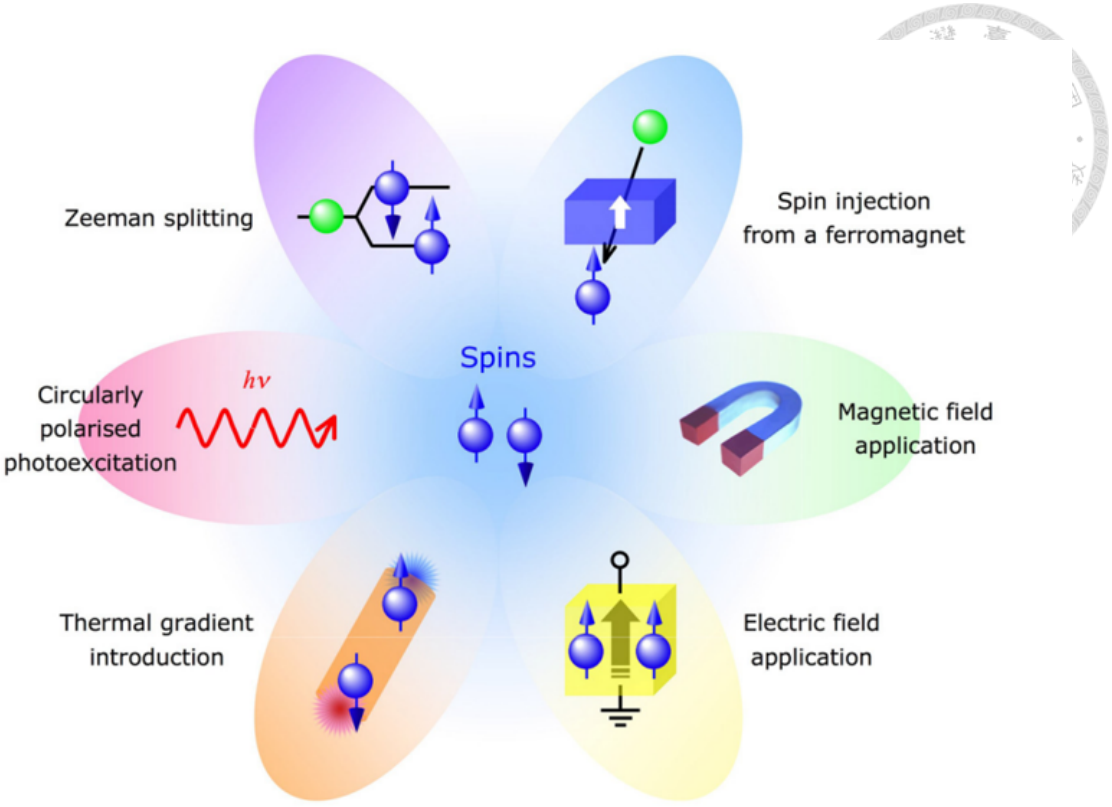

Figure 1.1: Spin-related physical phenomena.

In a spin valve, the relative alignment of the magnetic moments in the two ferromagnetic layers presents two distinct resistive states. When the magnetic moments are parallel, the device exhibits low resistance, allowing a high flow of spin-polarized electrons. Conversely, when the moments are antiparallel, the resistance increases, impeding the flow of electrons (Figure 1.2). This change in resistance is known as magnetoresistance (MR) and is the foundation of spin valve functionality. MR is defined as the eq 1.1

$$MR = \frac{R_{antiparallel} - R_{parallel}}{R_{parallel}} \tag{1.1}$$

Spin valves have diverse applications across various domains, with data storage standing out as one of the most significant areas of implementation. They serve as key components in magnetic read heads for hard drives, contributing to the advancement of high-density and high-capacity storage solutions.[4] Additionally, spin valves hold promise

doi:10.6342/NTU202400068

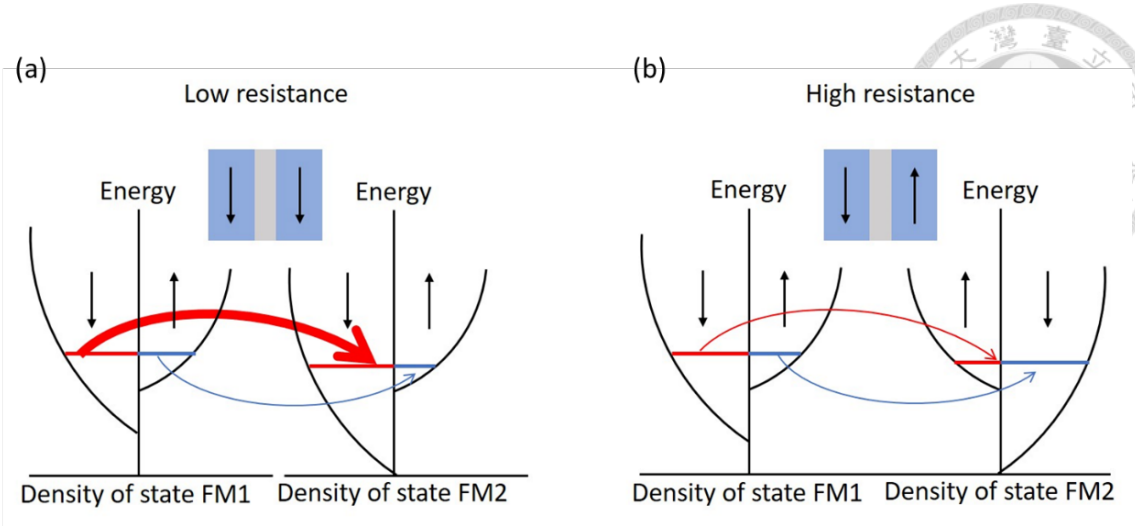

Figure 1.2: (a) The parallel spin alignment in spin valves creates low resistance, and (b) the antiparallel spin alignment creates high resistance.

in the development of spin-based logic devices and magnetic random-access memory (MRAM), where their ability to efficiently control the flow of spin-polarized electrons is leveraged. The spin valve utilized in MRAM is referred to as a magnetic tunnel junction (MTJ).

In the course of developing MTJ, commonly utilized insulating materials, such as Al_2O_3 and MgO, functioned as spacers. [5, 6] (Figure 1.3). However, as devices were scaled down, these materials exhibited increased defects and became rougher at the interface, leading to challenges like current leakage[7] and spin trapping[8].(Figure 1.4) Addressing these issues becomes crucial for the continued advancement and practical implementation of spintronics technology.

To conclude, spin valves represent a cornerstone in the fascinating world of spintronics. Their ability is expected to open up new avenues for faster, more efficient, and versatile electronic devices. As technological advancements progress, there is an increasing imperative to thoroughly unlock the potential of spintronics. This necessitates a heightened focus on exploring the applications of innovative materials and advancing our comprehension of the underlying mechanisms that govern spin transport.

doi:10.6342/NTU202400068

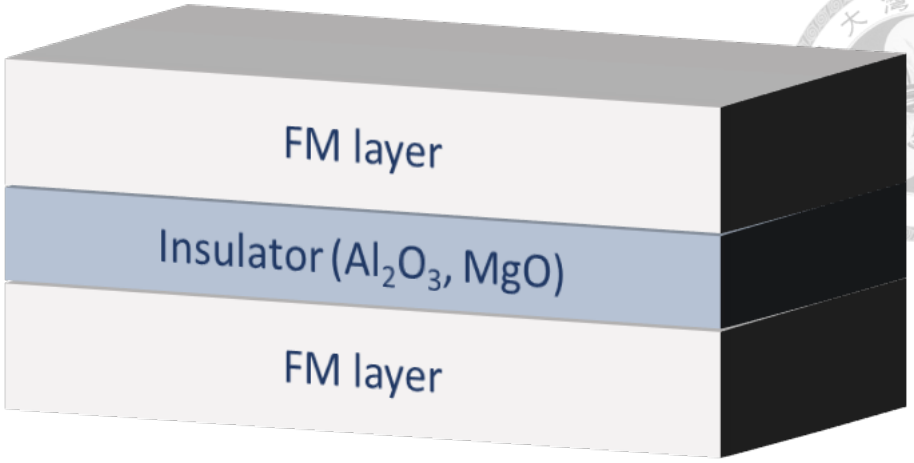

Figure 1.3: Traditional spin valves diagram using Al_2O_3 or MgO as spacers.

1.2 Two-dimensional materials in spintronic device

Two-dimensional materials (2DMs) present a promising avenue for overcoming the limitations of traditional materials for spacers due to their single-atom thickness, sharp interfaces[9, 10] (Figure 1.5), and precise control over thickness[11]. Hence, 2DMs are anticipated to play a critical role in advancing the miniaturization of components for spintronics.

Moreover, taking graphene as an example, it demonstrates superior spin filtering properties attributed to the appearance of a Dirac cone at the K point, contrasting with the gamma point predominant in common ferromagnetic materials.[12] (Figure 1.6). Consequently, only a minority of carriers can effectively traverse graphene. This spin-filtering effect provides a potential means to adjust the motion of electrons in the material by controlling their spin. Interestingly, graphene is renowned for its exceptional conductivity.[13, 14] However, it exhibits insulator-like behavior when electrons traverse in the vertical direction.[15] This opens up new possibilities for developing more efficient spin electronic components and devices, addressing some of the limitations encountered in traditional electronic devices.

doi:10.6342/NTU202400068

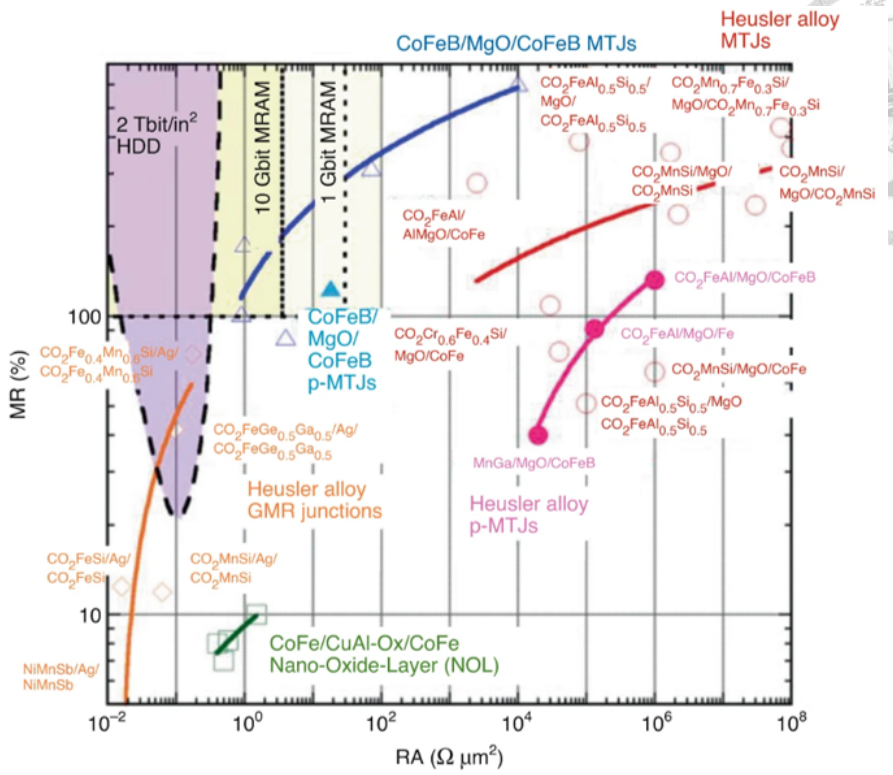

Figure 1.4: The development of spin valve-based devices

In addition to graphene, numerous other 2DMs showcase diverse properties. Multilayer graphene demonstrates a tunable electronic band structure as the layer count increases.(Figure 1.7) [16] Through precise thickness control, we can finely adjust the electrical properties from that of a conductor to a semiconductor.[17] MoS_2 is renowned for its excellent semiconductor characteristics, offering substantial potential applications in optoelectronic devices and energy conversion. Hexagonal boron nitride (h-BN) presents numerous advantages in the realm of spintronics. Beyond possessing mechanical strength comparable to graphene, h-BN inherently functions as an insulator. Intriguingly, the conductivity of graphene can be increased threefold by stacking it with h-BN[18]. The above only highlights a few characteristics of various 2DMs, and there are many more diverse materials that we cannot enumerate individually.

These diverse 2DMs not only exhibit unique properties but can also be finely tuned through layering, structural adjustments, chemical composition variations, and combina-

doi:10.6342/NTU202400068

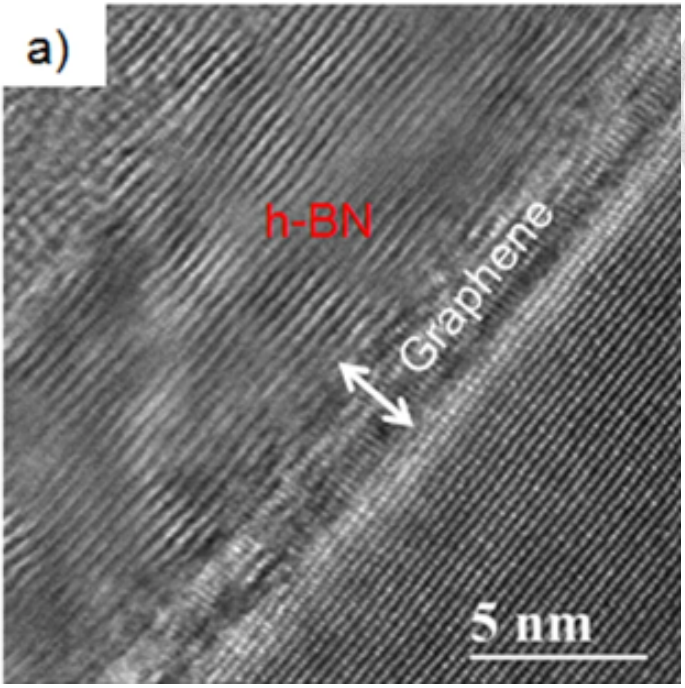

Figure 1.5: Sharp interface in 2D materials stack.

tions to meet the specific requirements of various applications. Consequently, the exploration of the use of 2DMs in spintronics holds significant value for advancing technological applications and enhancing our comprehension of the underlying physical mechanisms governing macroscopic behavior.

1.3 Interface effect

Until now, experimental realization of 2DMs-based barriers has fallen short of theoretical expectations, as evidenced by magnetoresistances below the anticipated values.[4, 19] (Figure 1.8) This disparity is often attributed to the low quality of interfaces between the spacer and ferromagnetic (FM) contacts, leading to reduced spin polarization.[20](Figure 1.9)

Efforts have been directed toward enhancing the interface quality, drawing inspiration from advancements in electronic coupling observed in transistors[21, 22]. One ap-

doi:10.6342/NTU202400068

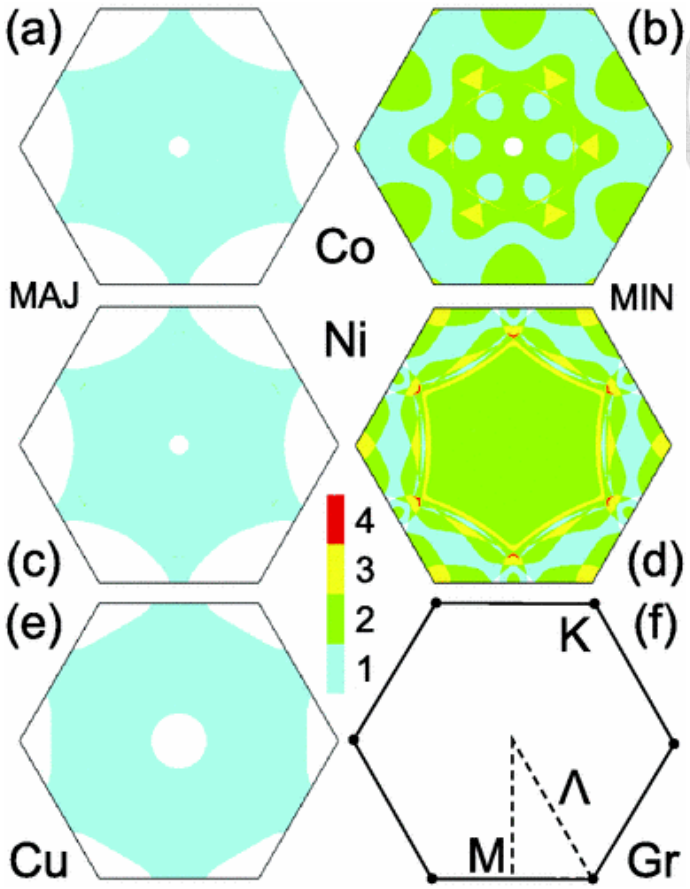

Figure 1.6: Energy band structure of common ferromagnetic materials, Co and Ni, and graphene.

proach to minimize oxidation at the interface involved the insertion of an Au film between the electrode and graphene by Mohiuddin *et al*. This extra layer successfully prevented oxidization during graphene transfer but came at the cost of reduced spin polarization[23], (Figure 1.10).

In a different strategy, Park *et al*. introduced a flip-transfer method to invert the graphene, aiming to enhance the intimacy of the contact/graphene interface. However, this manipulation of the exposed graphene interface heightened the risk of contamination and oxidation, potentially compromising the overall performance.[24] (Figure 1.11)

Attempting to streamline the process, Asshoff *et al* adopted a suspended membrane approach to decrease the number of processing steps, thus aiming to reduce the possibility

doi:10.6342/NTU202400068

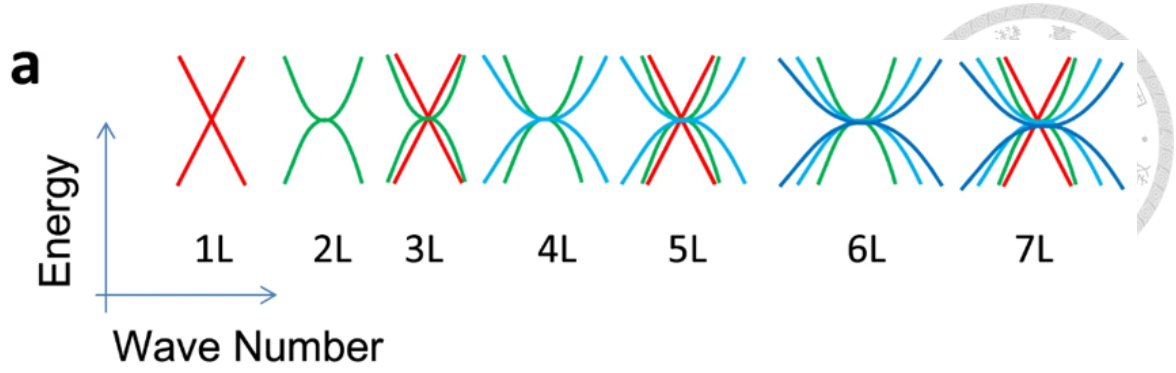

Figure 1.7: Thickness-dependent band structure in multilayer graphene.

of oxidation.[25] (Figure 1.12) However, despite this effort, the sequential evaporation still necessitated breaking the vacuum, leaving room for potential contamination. These results of MR are listed in Table 1

As of now, there is no established method to entirely avoid exposing the interface to ambient air and the inherent challenges associated with the transfer process of 2DMs.

1.4 Uninterrupted contact deposition method

We here demonstrate the potential of a novel approach that eliminates the processing steps that would deteriorate a 2D material's interface quality. In our "uninterrupted contact deposition (UCD)" scheme, ferromagnetic contacts with distinct properties are deposited on both sides of graphene without exposing the interfaces to the risk of contamination. To illustrate the potential of this method, ferromagnetic electrodes of asymmetrical thickness were deposited on both sides of the graphene all at once in a vacuum. (Figure 1.13)

Initially, porous mechanical support is precisely engineered, featuring patterns with diameters measuring just a few micrometers. The primary objective of this design is to facilitate the suspension of 2DMs. Subsequently, a rotary arm is integrated into the evaporator chamber, enabling the controlled rotation of our sample within the vacuum cham-

doi:10.6342/NTU202400068

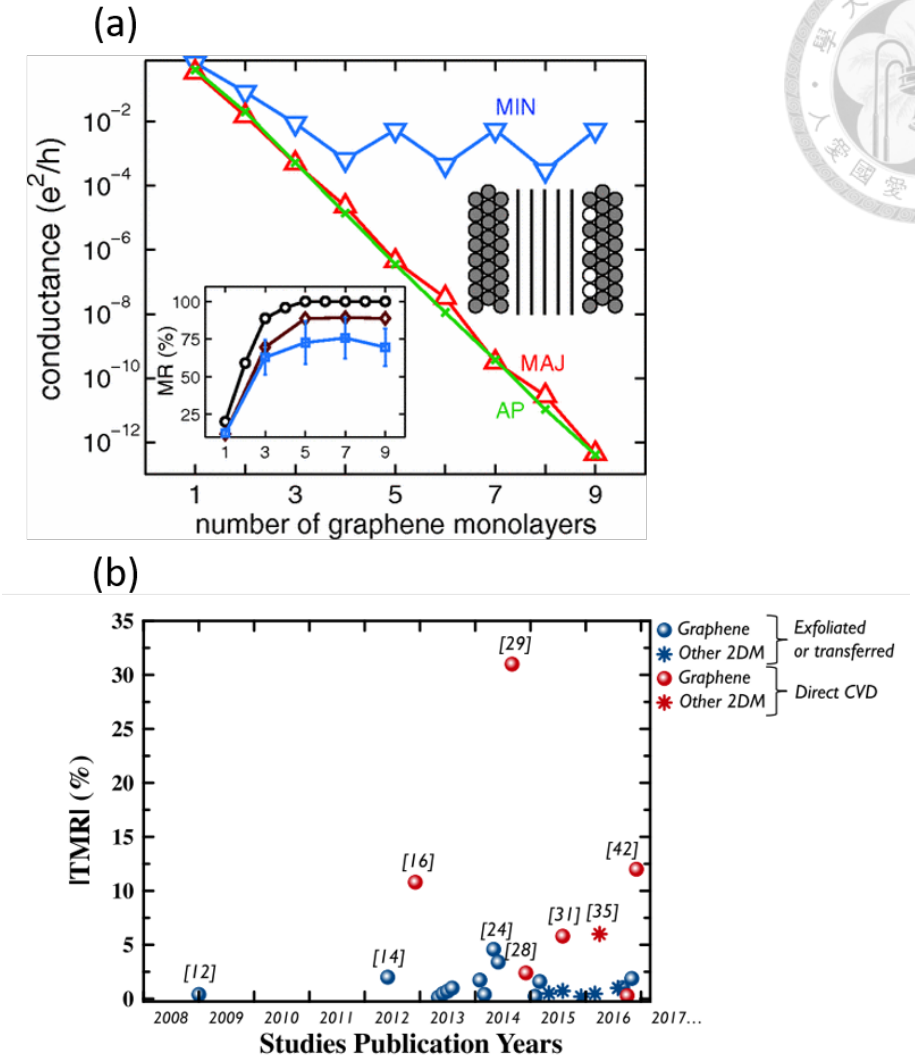

Figure 1.8: (a) Theoretical prediction for thickness-dependent MR in graphene spin valves with ideal(circle), middle(diamond), or rough interface(square), and (b) practical results about 2DMs-based spin valves.

ber, with the evaporator source originally positioned at the bottom. Lastly, ferromagnetic materials are deposited on both sides of the suspended 2DMs without compromising the vacuum integrity, thereby ensuring the highly clean interface within the spin valves.

This approach holds promise for streamlining and optimizing the fabrication process of spin valves with minimal steps. The specifics of the porous mechanical design are elucidated in the experimental section (Chapter 3).

doi:10.6342/NTU202400068

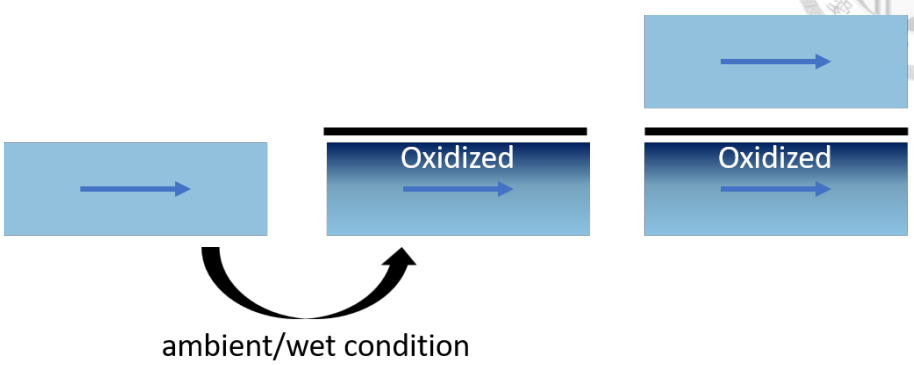

Figure 1.9: Oxidized problem on the interface as exposure to the ambient environment in the process of fabrication.

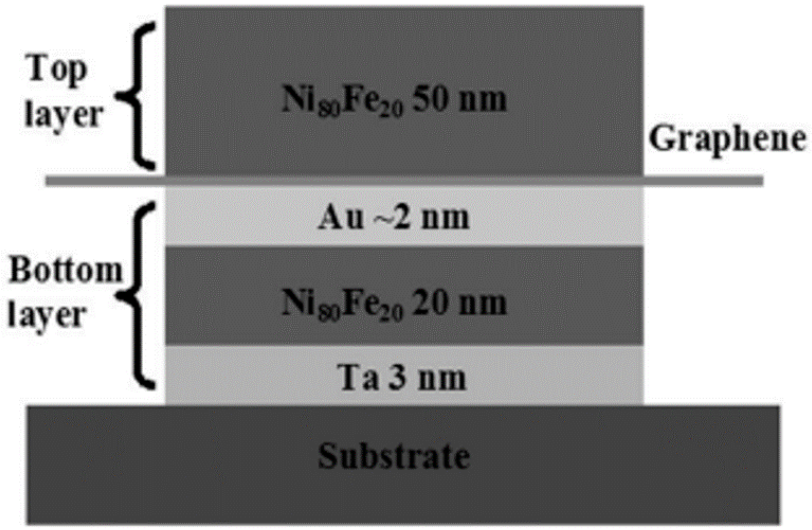

Figure 1.10: Utilizing the Au insert method to protect the surface of the bottom ferromagnetic electrode.

doi:10.6342/NTU202400068

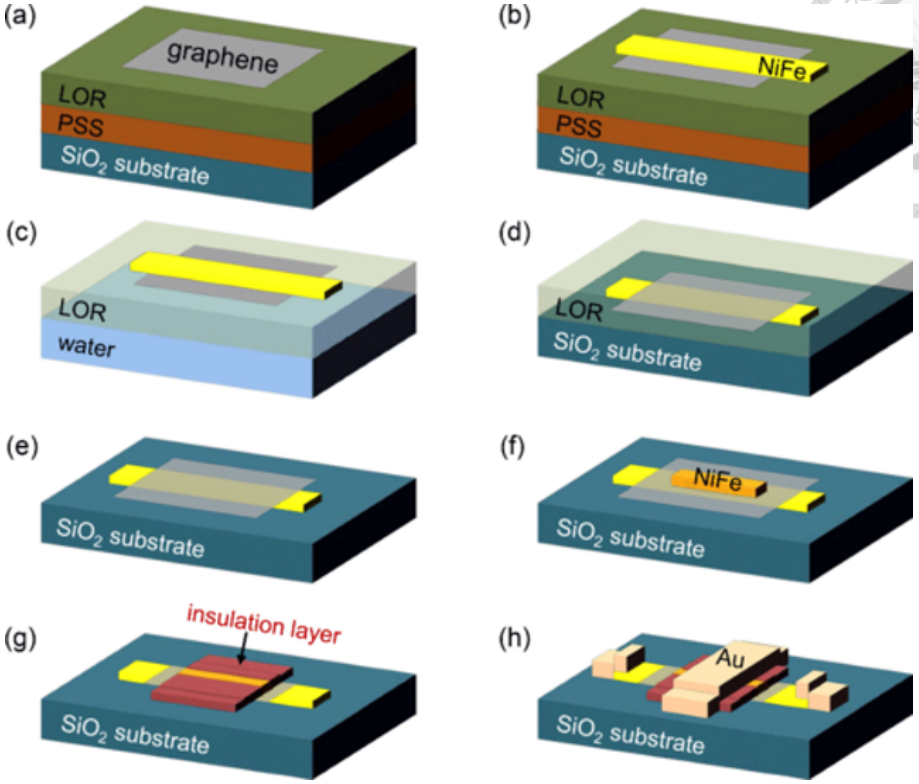

Figure 1.11: Utilizing the flipping method for the fabrication of spin valves

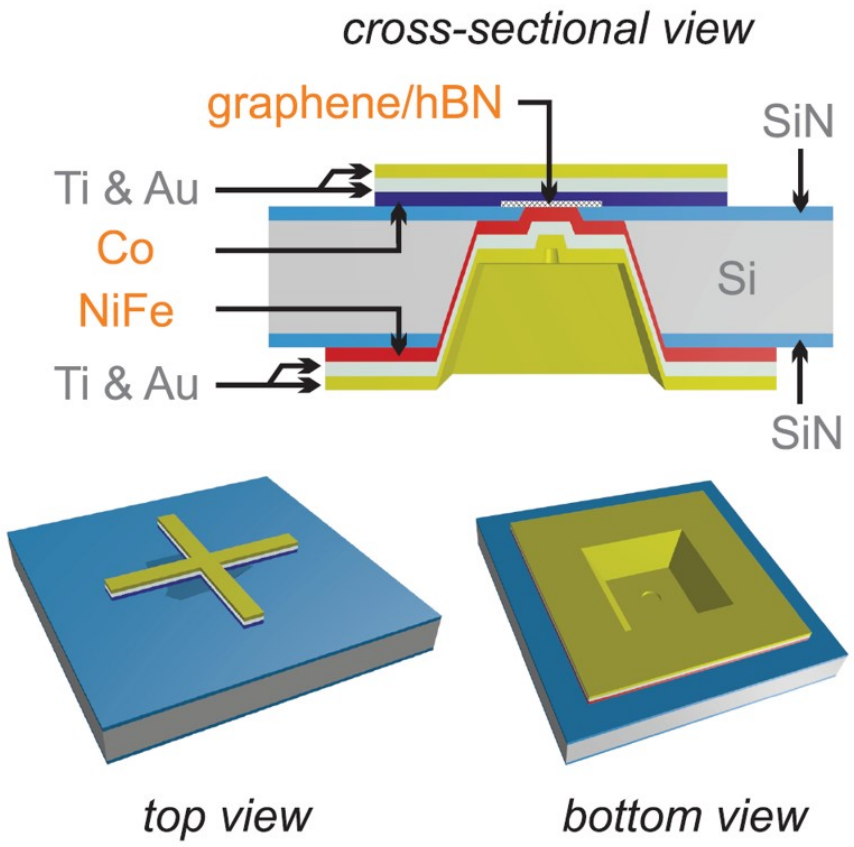

Figure 1.12: Utilizing the suspended method to fabricate spin valves.

doi:10.6342/NTU202400068

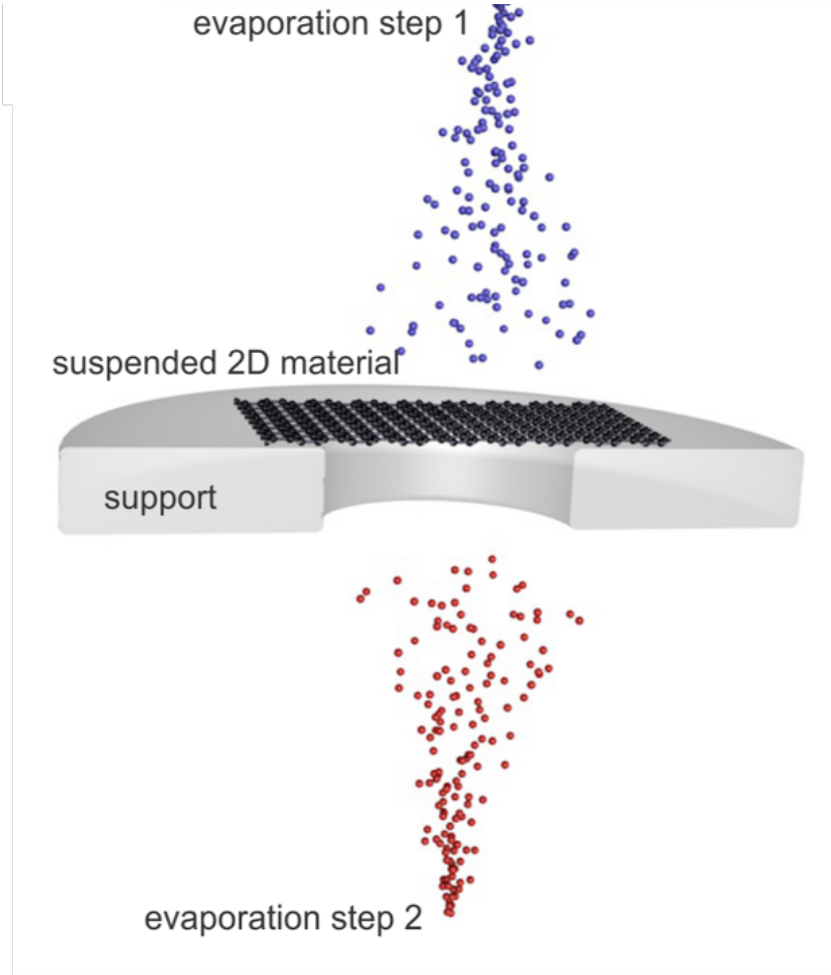

Figure 1.13: Diagram of the UCD method.

doi:10.6342/NTU202400068

Chapter 2 Theory

2.1 Electric characterization

Electric characterization plays a crucial role in spintronic devices, offering essential insights into their performance. It evaluates key parameters like spin transport efficiency, magnetoresistance, and electronic structure, guiding the fine-tuning and optimization of spin valves for advanced functionalities in next-generation electronic applications. Below, we will introduce several different relationships between current and voltage.

2.1.1 Ohmic contact

In the linear regime, the IV curve of a spin valve exhibits Ohmic behavior (Figure 2.1)[19]. This linear relationship between current (I) and voltage (V) is characterized by a constant resistance, indicating a well-established and predictable electrical response.[26] Ohmic contacts signify a straightforward flow of charge carriers, typically electrons, across the interface between materials, resulting in a linear IV curve. These contacts are crucial for efficient electron transport and are commonly desired in electronic devices. Ohmic behavior ensures a reliable and stable connection, facilitating consistent and controllable electrical responses in spin valves and other electronic components.

doi:10.6342/NTU202400068

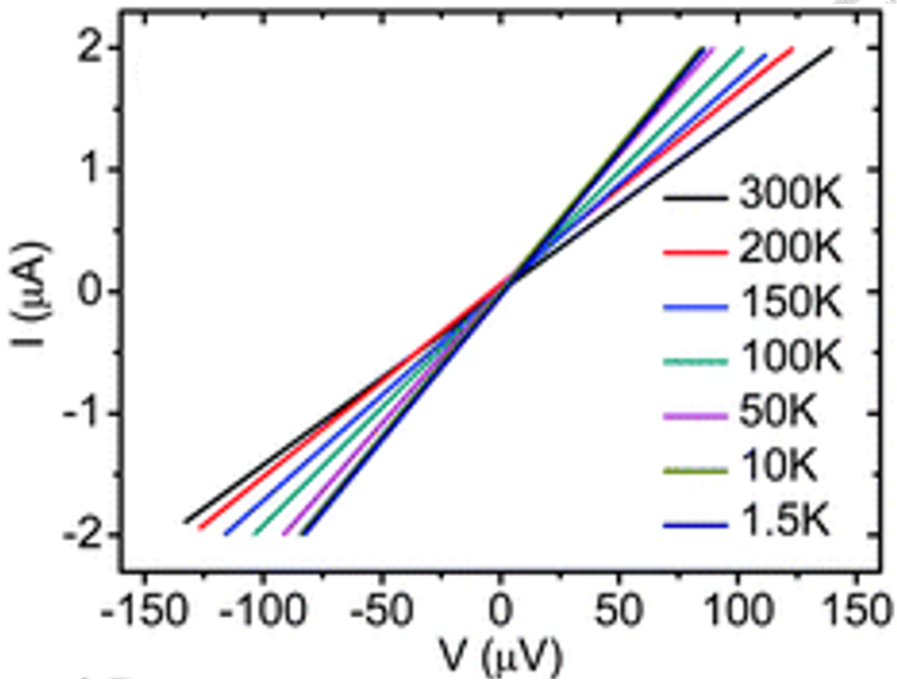

Figure 2.1: Electric properties of Ohmic contact.

2.1.2 Tunneling behavior

In this non-linear regime, the current-voltage (IV) curve departs from the linear relationship observed in Ohmic contacts, showcasing exponential increases in current with voltage.(Figure 2.2) The IV curve provides a distinctive profile that reflects the intricate interplay between quantum tunneling and the properties of the materials involved. This departure from Ohmic behavior is attributed to the influence of quantum mechanical tunneling, wherein charge carriers penetrate energy barriers between two electrodes.[27] The non-linear IV curve becomes a signature of tunneling-dominated transport, offering a unique window into the quantum nature of charge transfer in spin valves.

2.1.3 Direct tunneling

Direct tunneling occurs when charge carriers traverse a thin insulating barrier between two materials[28]. In the context of spin valves, this implies that electrons move

doi:10.6342/NTU202400068

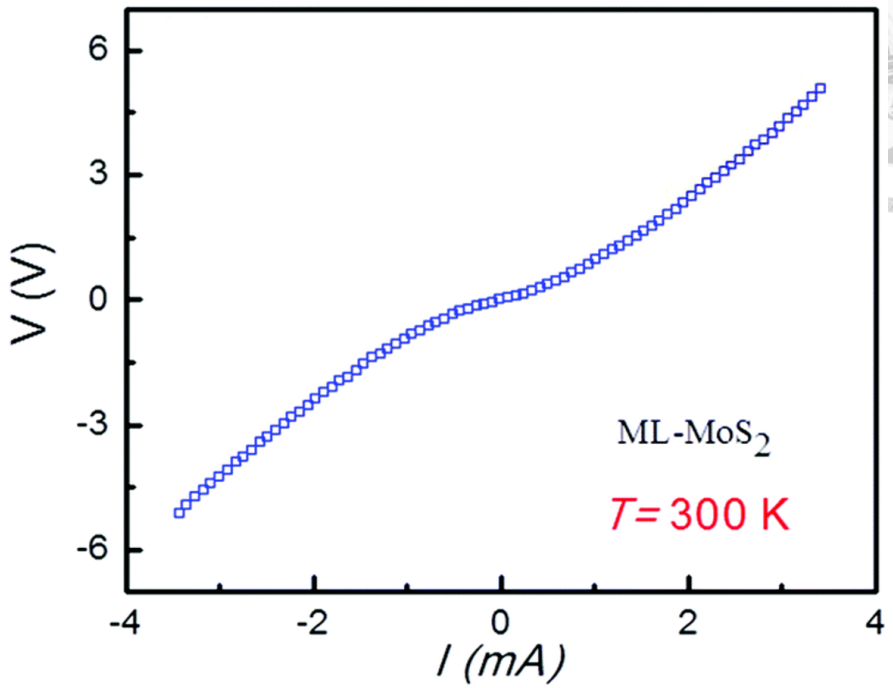

Figure 2.2: Electric properties of tunneling behavior.

through the insulating layer separating the ferromagnetic layers. Direct tunneling analysis involves the study of the tunneling probability, influenced by the thickness and properties of the insulating layer. The IV curve in this scenario reveals distinctive features, such as a rapid increase in current as the bias voltage surpasses the tunneling threshold. The description of this transport is shown in eq2.1 (Figure 2.3)

$$\ln \frac{1}{V^2} \propto \ln \frac{1}{V} (Direct tunneling) \tag{2.1}$$

$$\ln \frac{1}{V^2} \propto -\frac{1}{V} (FN tunneling) \tag{2.2}$$

doi:10.6342/NTU202400068

2.1.4 Fowler-Nordheim (FN) tunneling

Fowler-Nordheim (FN) tunneling is a crucial phenomenon observed in spin valves, particularly in devices characterized by a thicker insulating barrier.[28] Unlike direct tunneling, FN tunneling involves a more intricate process where charge carriers traverse the barrier through a quantum mechanical tunneling mechanism.

The IV curve during FN tunneling reveals distinctive features, with current increasing exponentially as the applied voltage surpasses a specific threshold. This threshold is intricately linked to the electric field strength and the characteristics of the insulating barrier. As voltage is incrementally applied across the thicker insulating layer in the FN tunneling regime, it allows charge carriers to surmount the energy barrier.(Figure 2.3)

The FN tunneling process is highly sensitive to variations in the electric field strength, making it a key parameter for understanding and manipulating the tunneling probability. Eq2.2 describes the behavior of the FN tunneling.

In summary, the current-voltage characteristics of spin valves offer valuable insights into their electrical behavior, with distinct regimes such as the linear (Ohmic contact) and non-linear (tunneling dominant) regions. The transition between these regimes is crucial in the design and optimization of spintronic devices. Furthermore, direct and FN tunneling analyses contribute to a nuanced understanding of the underlying mechanisms.

2.2 Magnetoresistance

Magnetoresistance (MR), a phenomenon ubiquitous in all metals, denotes the alteration of resistivity in response to a magnetic field. Classically, this effect is contingent

doi:10.6342/NTU202400068

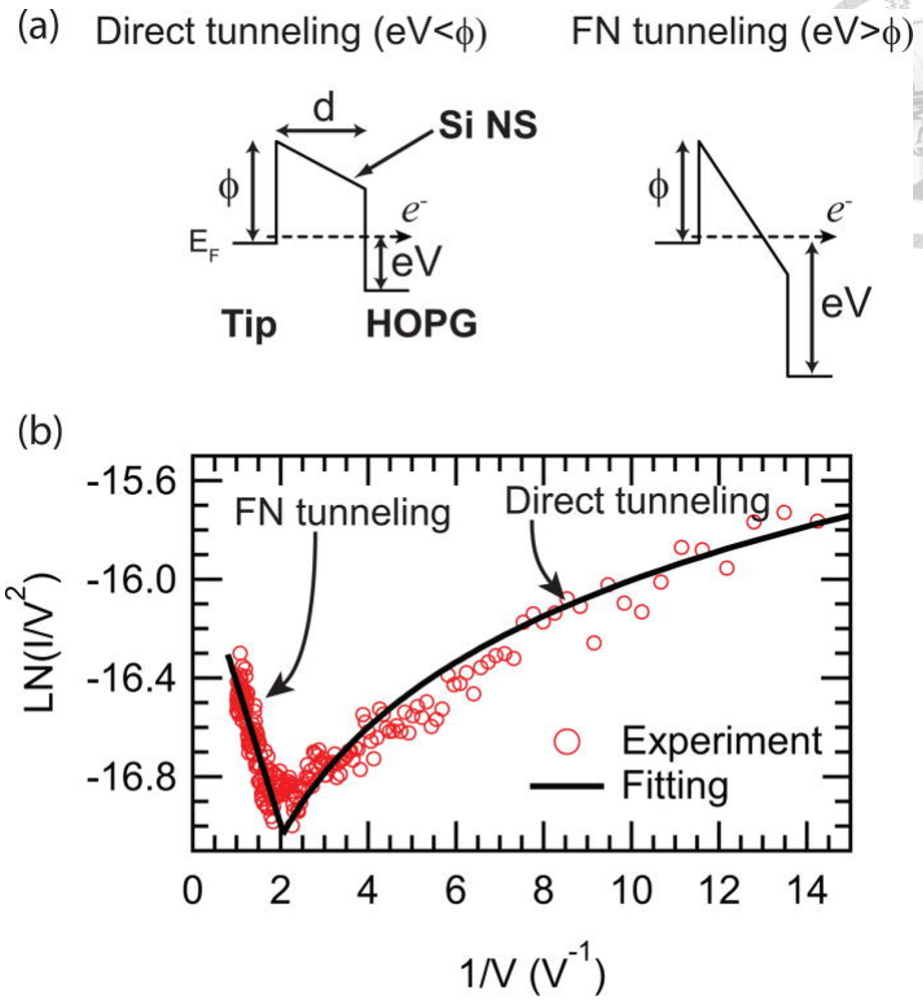

Figure 2.3: (a) Electron tunnels insulating energy barrier with different shapes and (b) the electric features of direct tunneling and FN tunneling.

upon both the strength of the magnetic field and the relative orientation of the magnetic field concerning the electric current. There are several distinct manifestations of magnetoresistance, each characterized by unique underlying mechanisms, including ordinary Magnetoresistance (OMR), anisotropic Magnetoresistance (AMR), giant Magnetoresistance (GMR), and tunneling Magnetoresistance (TMR).

2.2.1 Ordinary magnetoresistance (OMR)

OMR is a phenomenon observed in non-magnetic metals, where the resistivity increases with the application of an external magnetic field, both in parallel and perpendicu-

doi:10.6342/NTU202400068

lar directions. This enhancement is attributed to electrons deviating from the electric field direction under the influence of the Lorentz force. [29]

There are distinct cases of OMR behavior: Case1 demonstrates resistance saturation at high magnetic fields in metals like In, Al, Na, and Li; Case2 reveals magnetoresistance increasing with magnetic field up to the highest fields measured without dependence on crystallographic orientation in metals such as Bi, Sb, W, and Mo; Case3 describes metals like Cu, Ag, Au, and others, which exhibit large magnetoresistance in specific crystallographic directions due to Fermi surfaces with open orbit, while saturation occurs in other directions with closed orbits. [30]

The study of OMR provides insights into the interplay between magnetic fields and electrical conductivity in diverse metallic systems.

2.2.2 Anisotropic magnetoresistance (AMR)

AMR manifests in ferromagnetic metals such as Fe, Co, and Ni, where the resistivity undergoes distinct changes based on the orientation of an applied magnetic field.[29] Specifically, the resistivity increases when the magnetic field is parallel and decreases when it is perpendicular to the electric transmission. This phenomenon arises from spin-orbit coupling effects. When the magnetic field is perpendicular, it results in a small cross-section of electronic orbits, leading to low resistivity. Conversely, a parallel magnetic field creates a larger cross-section for scattering with electronic orbits, resulting in higher resistivity. (Figure 2.4) The interaction between magnetic field direction and electronic properties in ferromagnetic metals makes AMR a crucial aspect of understanding and manipulating material behavior for potential applications in electronic devices and

doi:10.6342/NTU202400068

technology.

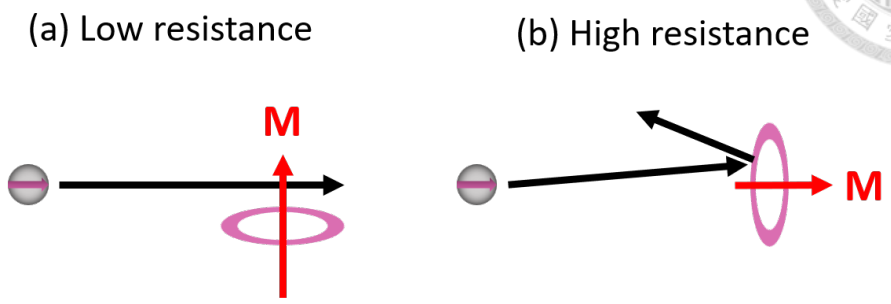

Figure 2.4: (a) The perpendicular alignment of magnetic field and electron transport induces a small cross-section, and (b) the parallel alignment of magnetic field and electron transport induces a large cross-section.

2.2.3 Giant magnetoresistance (GMR)

Giant Magnetoresistance (GMR) is a remarkable phenomenon observed in materials with aligned ferromagnetic layers. The foundation of GMR lies in the spin-valve structure, FM/non-FM conductor/FM where the relative alignment of magnetic layers profoundly influences electron transport properties.(Figure 2.5) In a parallel alignment, the current is predominantly carried by a certain spin direction, facilitating their smooth passage through the material with weak scattering, resulting in a lower resistance state.[31] Conversely, in an anti-parallel alignment, both spin-up and spin-down electrons experience stronger scattering in the process of transport. This configuration leads to an overall higher resistance. (Figure 2.6) This extraordinary sensitivity to magnetic alignment makes GMR an element in the development of advanced technologies, particularly in the design and optimization of magnetic sensors and data storage devices.

doi:10.6342/NTU202400068

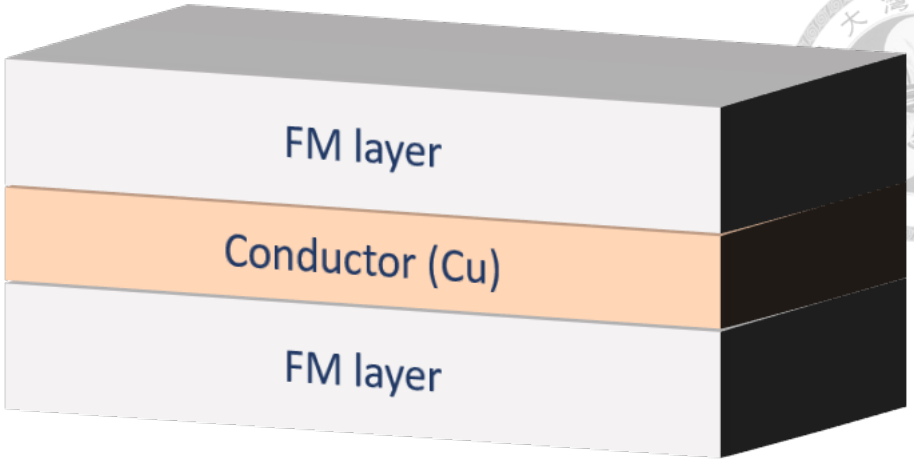

Figure 2.5: Diagram of GMR spin valves.

2.2.4 Tunnel magnetoresistance (TMR)

Tunneling Magnetoresistance (TMR) is a phenomenon observed in structures employing a FM/insulator/FM configuration. The TMR effect is contingent upon the orientation of magnetization and correlates with the spin polarization of tunneling electrons traversing insulating barriers.[6] In comparison to GMR, the alteration in magnetoresistance remains consistent based on magnetic orientation, yet the mechanism of carrier transport varies across different spacers, conductors, and insulators, respectively.

In conclusion, the exploration of magnetoresistance phenomena, including OMR, AMR, GMR, and TMR, unveils the intricate relationship between magnetic fields and electrical conductivity in diverse metallic systems. Each manifestation offers unique insights, from electron deviation under Lorentz force in OMR to spin-orbit coupling effects in AMR, and aligned magnetic layers in GMR. TMR, relying on tunneling through insulating barriers, presents a distinctive mechanism. A comprehension of these diverse magnetoresistance mechanisms aids in the investigation of spintronics devices.

doi:10.6342/NTU202400068

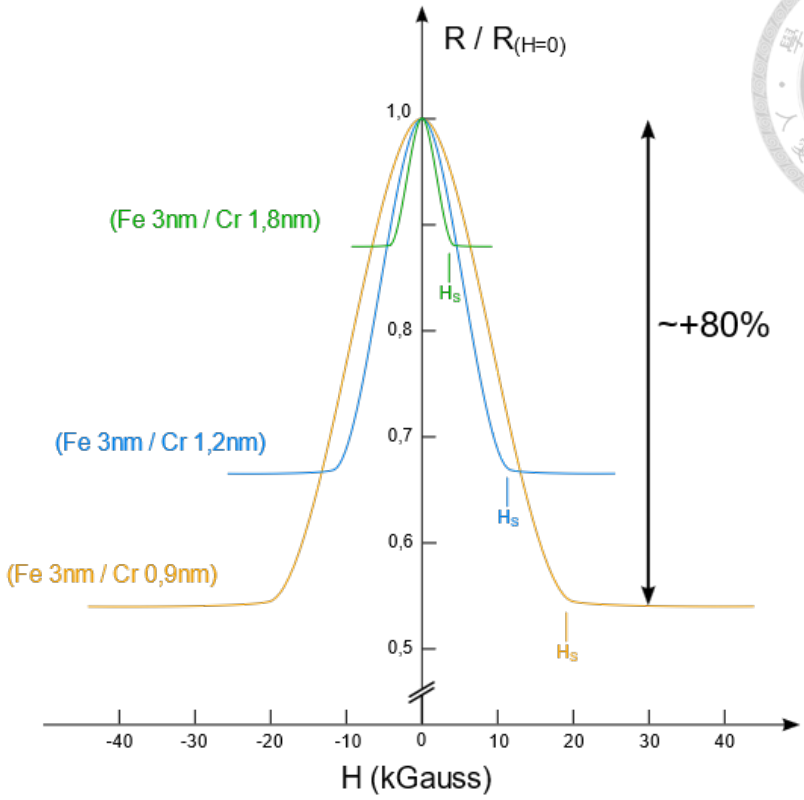

Figure 2.6: Giant magnetoresistance variation in spin valves in response to magnetic field changes.

2.3 Hanle effect

The Hanle effect is a phenomenon observed in spin-polarized systems when a spin-polarized population of carriers is subjected to an external magnetic field. Spin-transport parameters can be derived through the utilization of the Hanle effect. In this phenomenon, a magnetic field is applied perpendicular to the direction of spin accumulation, leading to the precession and dephasing of spins within the lateral channel.[32](Figure 2.7)

The spatial spread of the spin polarization in a material is characterized by the spin diffusion length l_{sf} which is related to the spin-lattice relaxation time τ_{sf}. Fitting the Hanle curves with solutions of Bloch equations[33] is particularly useful for studying spin

doi:10.6342/NTU202400068

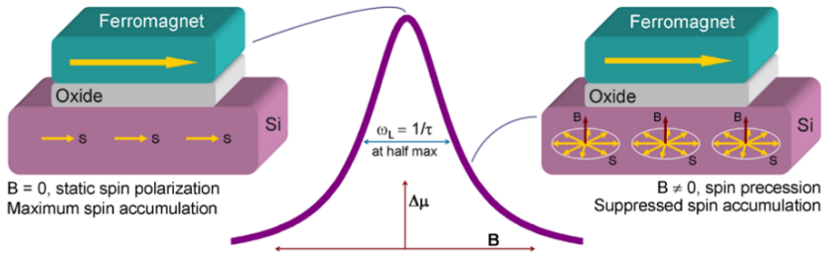

Figure 2.7: This explains the mechanism by which a perpendicular external magnetic field relaxes the spin accumulation at the interface.

relaxation times and spin coherence lengths in semiconductors and other materials.

$$l_{sf} = \frac{D}{{\tau_{sf}}^2} \tag{2.3}$$

In the absence of a magnetic field, the accumulation of spin electrons at the spin valve interface results in induced voltage. However, when an external perpendicular magnetic field is applied, the relaxation of spin accumulation leads to a decrease in voltage within the spin valve. [33, 34]This phenomenon can be mathematically described by the following equation eq 2.4

$$\delta V(B \perp) = \frac{\delta V(0)}{1 + (tw_L)^2} \tag{2.4}$$

, where V is the voltage difference caused by spin accumulation, ω_L is the Larmor precession frequency. [34]

The Elliot-Yafet (EY) and Dyakonov-Perel (DP) mechanisms are two commonly employed models for studying spin transport in materials.[35] EY proposes that spin-orbit coupling has the potential to induce spin information loss, resulting in a spin lifetime proportional to the momentum scattering time. Additionally, EY suggests that the spin lifetime increases with the number of graphene spacer layers due to improved screening

doi:10.6342/NTU202400068

of external scattering potentials.[35]

On the other hand, DP associates spin flips with the accumulation of lattice-induced precession of spin between scattering events. Furthermore, DP emphasizes that the spin lifetime corresponds to the fastest relaxation pathway.[35] Consequently, relaxation can occur through spin escape to the electrodes, where the relaxation is much faster. As a result, the critical trade-off of contact resistance becomes imperative in the design of spin valves.

doi:10.6342/NTU202400068

doi:10.6342/NTU202400068

Chapter 3 FABRICATION PROCESS AND EXPERIMENTS SETUP

3.1 Porous mechanical support

The preparation of porous mechanical support is a critical step to achieve UCD methods to suspend 2DMs.

Our UCD approach relies on two advances, firstly, the 2D material is suspended to expose both interfaces. Secondly, contacts are deposited on both sides in a process without breaking any vacuum until completion. Therefore, the preparation of a porous mechanical is necessary in the initial stage.

Figure 3.1 illustrates the preparation process. To begin, a 500 nm low-stress silicon nitride (SiN) layer was grown on both sides of a 200 μm silicon wafer. Subsequently, employing photolithography techniques and a double-side optical mask aligner, squares with 500 μm sides were designed for the bottom window, while circles with diameters ranging from 3 to 5 μm were configured for the top window. The optical masks' patterns are depicted in Figure 3.2, with further elaboration on each pattern provided in Figure 3.3

doi:10.6342/NTU202400068

for a more detailed view.

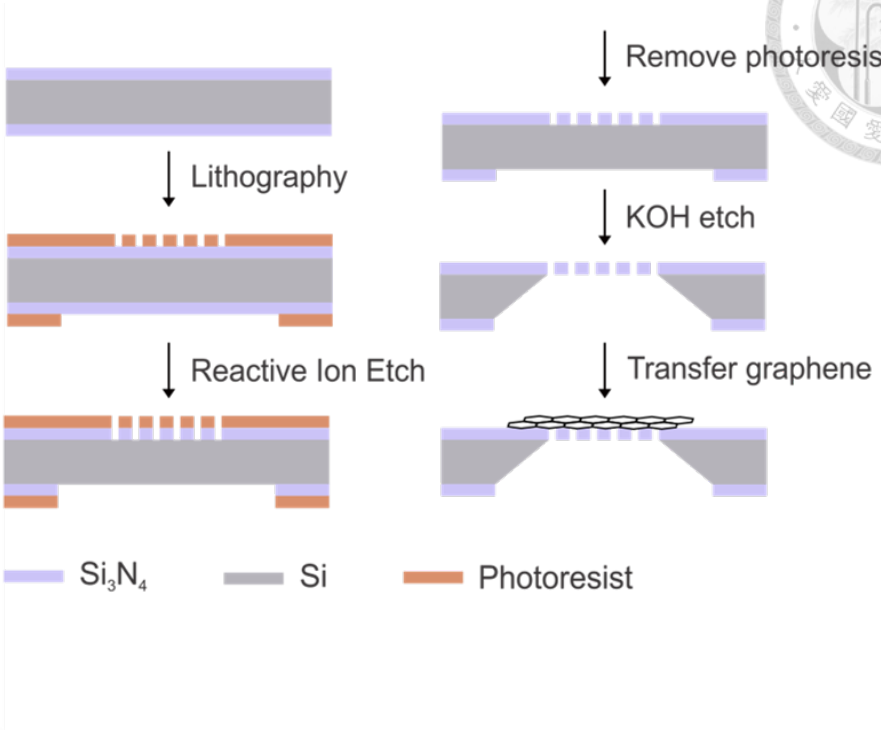

Figure 3.1: The procedure for fabricating the porous mechanical support to suspend 2D materials.

Following that, a reactive ion etch (RIE) was employed to remove the designated patterns on the silicon nitride at a rate of 47.1 per minute. Ultimately, the complete wafer underwent immersion in a 30 wt% KOH solution at 80°C for several hours, facilitating thorough penetration from the top to the bottom. The cross shapes on both sides serve as markers for dual-sided alignment.

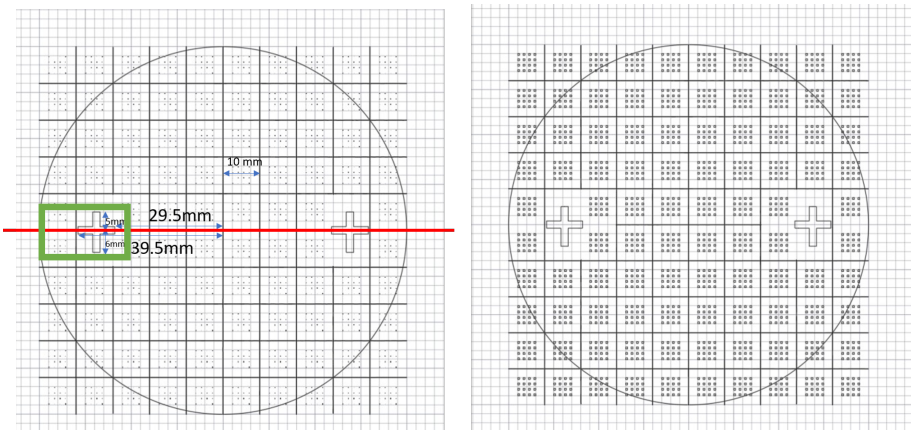

Figure 3.2: (Left) Top pattern and (Right) bottom pattern on the optical mask

doi:10.6342/NTU202400068

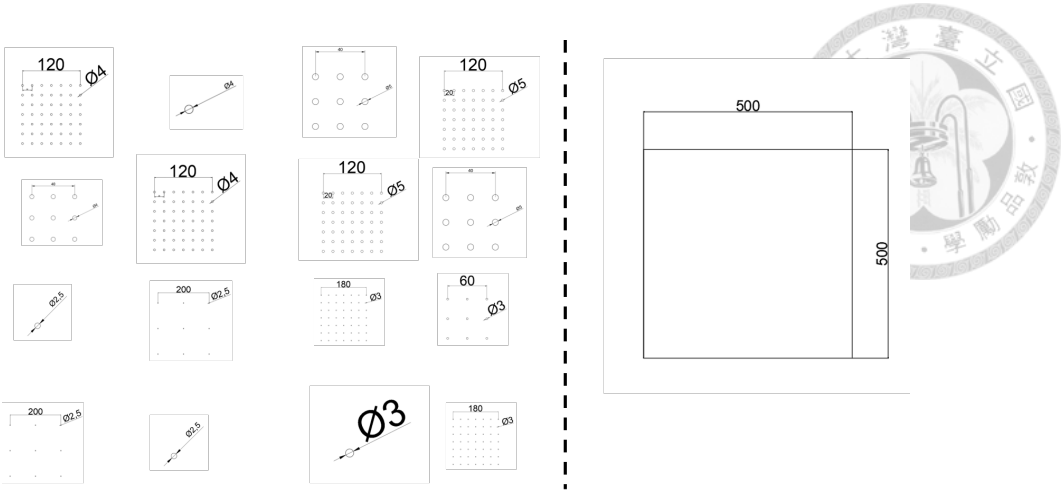

Figure 3.3: (Left) Top pattern and (Right) bottom pattern on the optical mask or a more detailed view.

3.2 2D materials transfer method and thermal decomposition

Graphene was transferred onto the porous mechanical support employing a wet transfer technique. Initially, a layer of polymethyl methacrylate (PMMA) was spin-coated onto the graphene-coated copper foil at a rate of 2500 rpm. Subsequently, the sample underwent immersion in ammonium persulfate to selectively etch away the copper foil, followed by multiple rinses in deionized water to ensure thorough cleanliness. The resulting floating membrane was delicately lifted and affixed onto the porous mechanical support. To minimize residual PMMA, thermal decomposition was applied to the sample at a temperature of 400°C.[36] This thermal treatment involved a flow of 200 sccm of hydrogen (H_2) and 200 sccm of argon (Ar) for a duration of 1 hour. Subsequently, the sample was allowed to cool naturally inside the oven.

doi:10.6342/NTU202400068

3.3 Photolithography

Photolithography is a fundamental technique in microfabrication and semiconductor device manufacturing. It involves a process of transferring a pattern onto a substrate using light-sensitive materials. A photosensitive resist is first coated onto the substrate. Then, a mask containing the desired pattern is placed over the resist-coated substrate. When exposed to ultraviolet light, the resist undergoes a chemical change, creating a patterned mask. Subsequent development steps remove either the exposed or unexposed regions, leaving behind the desired pattern on the substrate. The spin valve pattern fabricated by conventional methods is designed primarily by photolithography. (Figure 3.4)

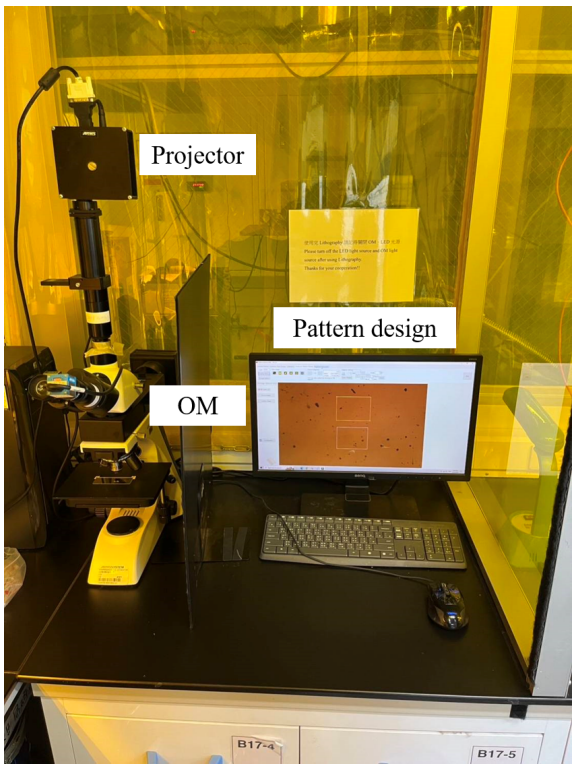

Figure 3.4: Photolithography system.

doi:10.6342/NTU202400068

3.4 E-beam evaporator

The e-beam evaporator is a sophisticated thin-film deposition system employed in the fabrication of various electronic devices evaporator (AST E-GUN PEVA-600I). Its fundamental working principle involves the generation and controlled manipulation of a high-energy electron beam to vaporize a material source, allowing for the deposition of a thin film onto a substrate. (Figure 3.5)

In our system, the vacuum is maintained at 10^{-6} torr throughout the fabrication process. The deposition rate is held constant at 0.1 Å/s to ensure the quality of the electrode. Additionally, a rotary arm has been installed in the chamber to facilitate the implementation of the UCD method (Figure 3.6).

Figure 3.5: E-beam evaporator system.

doi:10.6342/NTU202400068

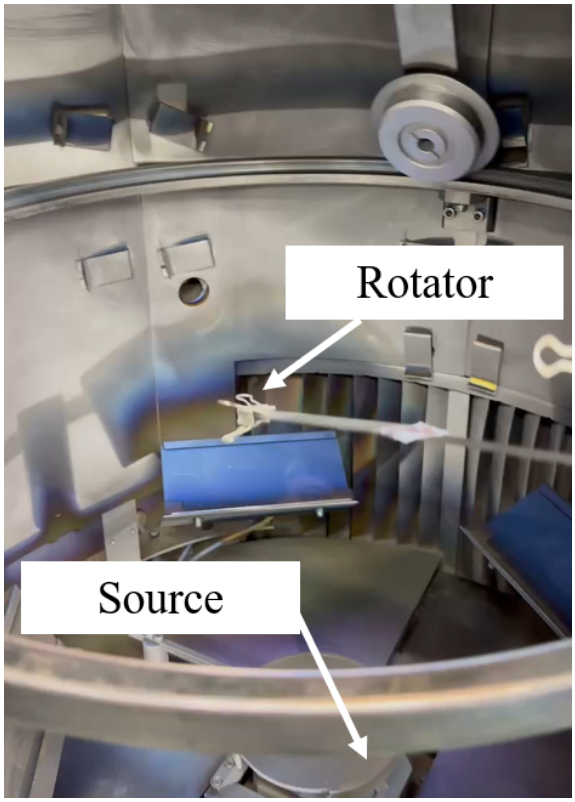

Figure 3.6: E-beam evaporator system installed with a rotary system

3.5 Raman spectroscopy

Raman spectroscopy was conducted with a 532 nm excitation source in a Nanobase XPER RF.

Raman spectroscopy is a process of photon-in and photon-out, (Figure 3.7) wherein photons of a specific energy are directed into a material. Photon-molecule interaction is an inelastic scattering process. The interaction of these photons with different molecules causes them to lose certain energy. By detecting the energy of photo-out, the feature of materials can be identified.

Within materials, atoms oscillate near their equilibrium positions and variations in structure cause stretching or distortion of the atomic bonds. These phenomena result in the emission of unique vibrational frequencies, analogous to individual human fingerprints.

doi:10.6342/NTU202400068

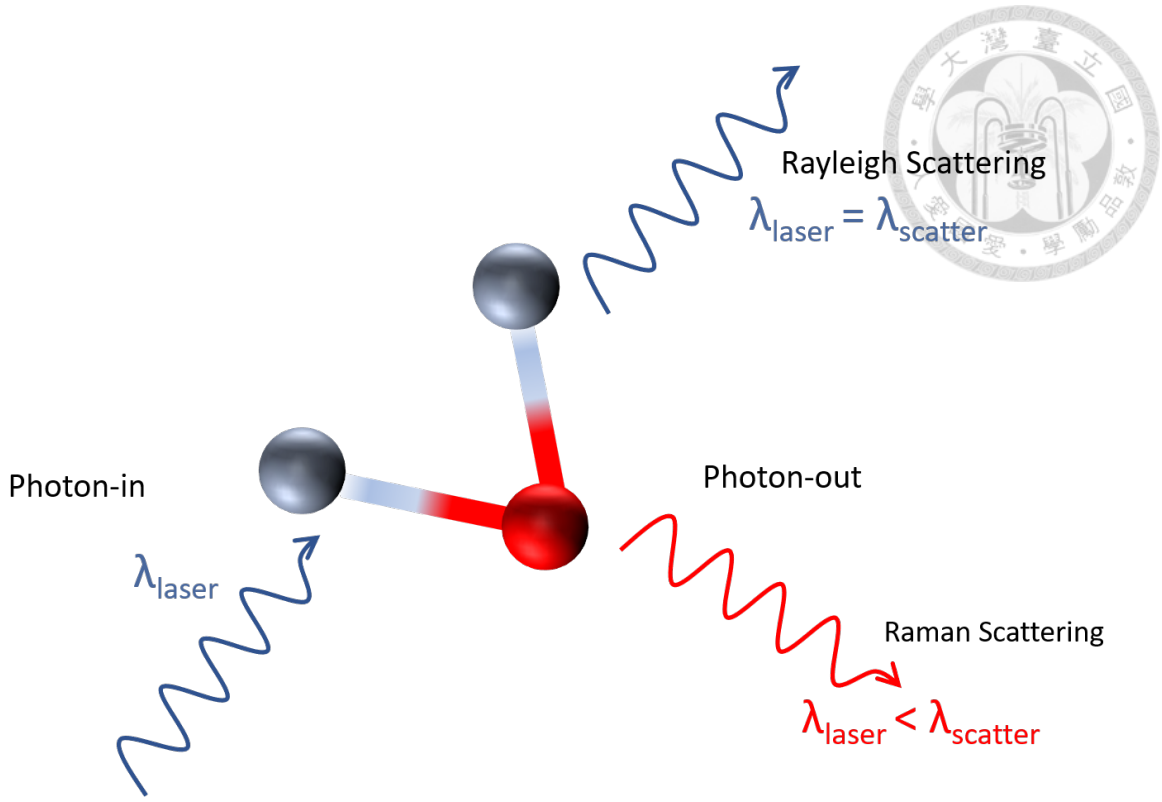

Figure 3.7: The photon-in and photon-out process in Raman spectroscopy.

When light interacts with the molecular vibrations in a material, it undergoes distinctive energy changes, serving as a basis for the identification of different materials.

In Raman spectroscopy experimental results, the X-axis is typically presented as the reciprocal of wavelength, as the reciprocal of wavelength is directly proportional to energy. This facilitates scientists in interpreting the energy changes after photon scattering. The Y-axis represents scattered light intensity, which is related to the observed molecular vibrational modes. A higher intensity of scattered light indicates a higher proportion of existing vibrational modes, allowing inferences about the quality of the material structure. However, unexpected signals in regions where peaks are not anticipated could indicate contamination in the sample.

When analyzing graphene using Raman spectroscopy, characteristic peaks appear around 1580 cm^{-1} and 2680 cm^{-1}.[37] These peaks correspond to the planar vibration of graphene and the resonance of photons generated in graphene, respectively. By studying

doi:10.6342/NTU202400068

the relative intensity and position of these two peaks, further exploration of other characteristics of graphene is possible.

If the intensity of the two characteristic peaks is weak, it suggests the presence of defects in graphene. If the 1560 cm^{-1} peak is relatively strong and the 2680 cm^{-1} peak becomes weaker, it may indicate the presence of multilayer graphene.[38]

Our Raman spectroscopic measurement was conducted with a 532 nm excitation source in a Nanobase XPER RF.

3.6 Surface and interface characterization

3.6.1 Atomic force microscopy (AFM)

Atomic Force Microscopy (AFM) is a powerful imaging technique that enables the visualization of surfaces at the atomic and molecular levels. The fundamental working principle of AFM involves the use of a sharp tip attached to a flexible cantilever to scan a sample surface. As the AFM tip approaches the sample surface, various forces come into play. (Figure 3.8) The primary forces involved include van der Waals forces, electrostatic forces, and repulsive forces between atoms. [39]

The interaction forces cause the cantilever to deflect or bend. The degree of deflection is directly related to the forces acting between the tip and the atoms on the sample surface.

AFM offers versatile imaging modes. In contact Mode, the tip continuously contacts the sample, providing high-resolution images but may wear the tip and sample. Tapping Mode oscillates the tip, reducing lateral forces for softer samples. Non-contact mode

doi:10.6342/NTU202400068

hovers the tip without direct contact, minimizing potential damage.

In our research, AFM plays an essential role in characterizing suspended graphene. To safeguard the integrity of the graphene, we exclusively utilize the non-contact mode for all our scanning procedures, thereby ensuring that no harm is imposed during the imaging process.

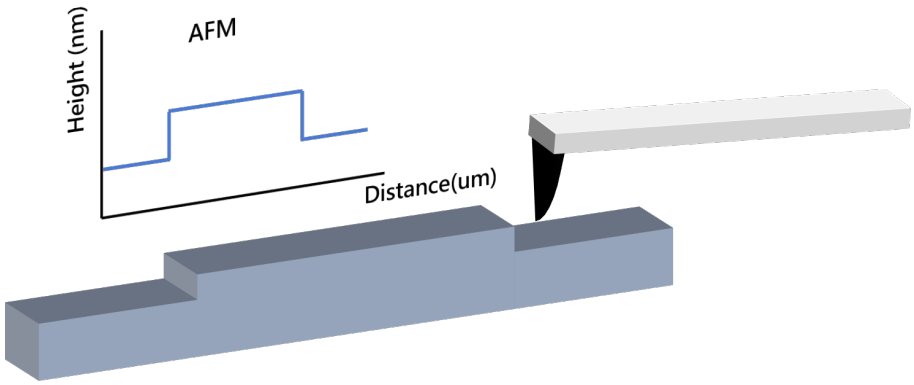

Figure 3.8: Diagram illustrating the AFM process.

3.6.2 Scanning electron microscopy (SEM)

Scanning Electron Microscopy (SEM) is an imaging technique widely used for high-resolution characterization of surfaces. SEM utilizes an electron gun to generate a focused beam of high-energy electrons. These electrons are accelerated towards the sample with energies typically ranging from a few kilovolts to tens of kilovolts.[39]

As the electron beam interacts with materials, resulting in the emission of various signals. The primary interactions include elastic scattering, inelastic scattering, and secondary electron emission. [39]

Some electrons within the incident beam undergo elastic scattering, known as backscattering. The energy and intensity of the backscattered electrons provide information about the sample's atomic composition. Inelastic scattering can cause the ejection of secondary

doi:10.6342/NTU202400068

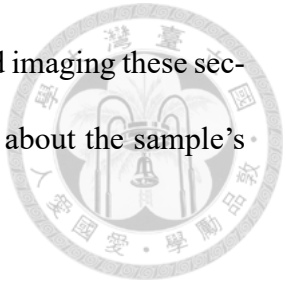

electrons from the sample surface. SEM often focuses on detecting and imaging these secondary electrons, as they provide detailed topographical information about the sample's surface features.

Detectors capture the emitted electrons and convert them into signals that are then used to generate high-resolution images of the sample surface. The resulting images reveal surface morphology, topography, and compositional information.

Furthermore, the SEM system, coupled with Focused Ion Beam (FIB) technology, facilitates accurate milling, cutting, and imaging of samples at the nanoscale. This enables a meticulous investigation into the cleanliness of interfaces through a controlled and destructive study. The SEM procedures presented in our results were performed at the Instrumentation Center in National Taiwan University, utilizing the FEI Helios600i FIB system.

3.6.3 Energy-dispersive X-ray spectroscopy (EDX)

Energy-dispersive X-ray spectroscopy (EDX) is an analytical technique commonly utilized in electron microscopy to elucidate the elemental composition of materials. The fundamental operation of EDX involves a series of key steps.

When a high-energy electron beam interacts with a sample in an electron microscope, it induces inner-shell electrons to escape from atoms, creating vacancies in the original position. To regain stability, outer-shell electrons may transition, emitting characteristic X-rays.

Each element produces characteristic X-ray peaks at specific energy levels, allowing for elemental identification. The spectrum is analyzed by comparing peaks with known

doi:10.6342/NTU202400068

standards. This qualitative analysis provides valuable insights into the elemental composition of the sample.

3.7 Magnetoresistance measurement

The study of magnetic response is primarily conducted within Professor Chuang's laboratory utilizing a low-temperature closed cycle magnetoresistance measurement system, as illustrated in Figure 3.9.[40] All measurements are conducted within a high vacuum environment, sustaining a pressure level of 10^{-6} torr.

The system facilitates a temperature-dependent investigation spanning the range of 4.6K to 420K. Notably, the system's capacity to achieve elevated temperatures allows for the annealing of measured samples, enabling a comparative analysis of their characteristics before and after this thermal treatment.

The applied magnetic field can vary from -1 T to 1 T in either perpendicular or horizontal orientations, thereby providing a substantial range beneficial to the examination of universal electronic devices and the elucidation of anisotropic properties. For electric and magnetic measurements, the system employs a Keithley 2400 source meter and an AC lock-in amplifier to collect the response of devices.

doi:10.6342/NTU202400068

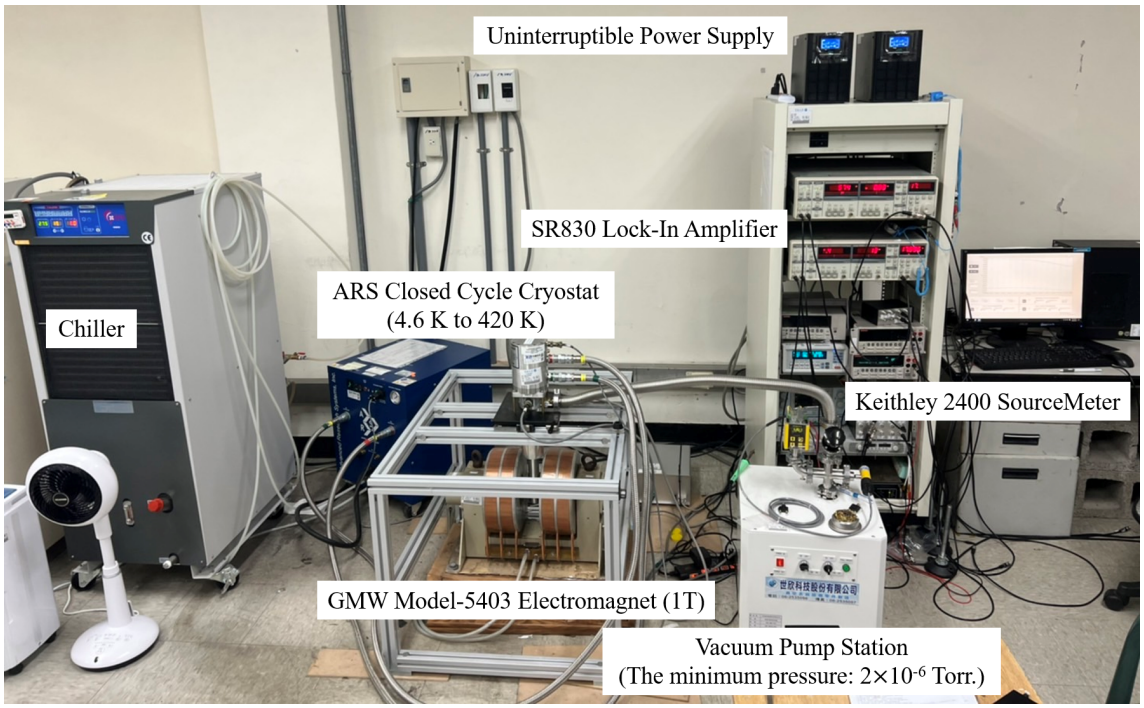

Figure 3.9: Magnetic properties measurements in CYCU.

doi:10.6342/NTU202400068

Chapter 4 Result and Discussion

4.1 Realizing high-quality interfaces in 2DMs spin valves

4.1.1 Characterization

Raman spectroscopy is employed to investigate the properties of suspended graphene. The continuity of suspended graphene is supported by Raman spectroscopic mappings that show the retention of the G-band feature at the opening. (Figure 4.1a)[41] Compared to the supported region, the suspended graphene part exhibits a downshifted G-band feature indicating the relaxation of transfer-induced tensile strain. (Figure 4.1b)[41]

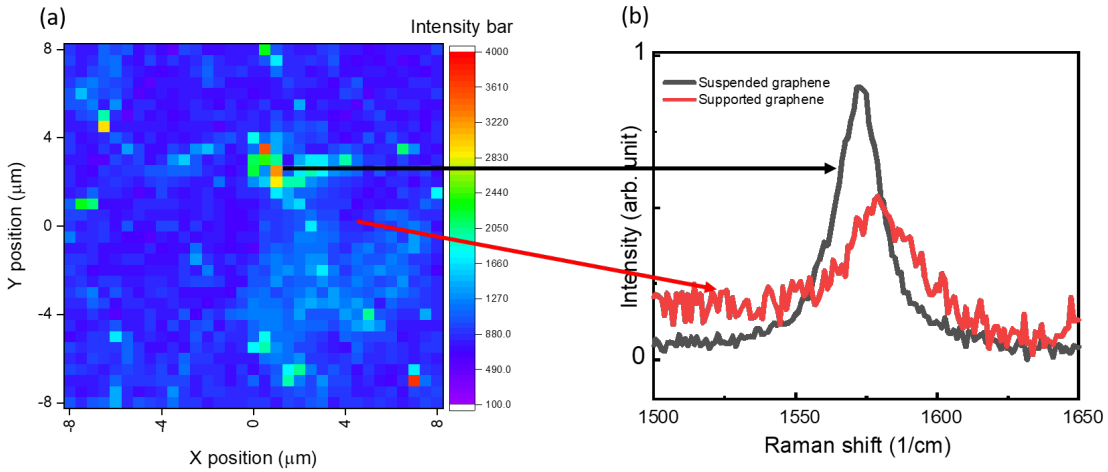

Figure 4.1: (a) Raman mapping on the suspended and the supported graphene, and (b) the respective spectrum from the suspended and the supported graphene.

We confirmed the structural integrity of suspended graphene through AFM mapping.

doi:10.6342/NTU202400068

The presence of graphene on holes was revealed in all devices, underscoring the effectiveness of our graphene transfer method and poly-support removal in achieving complete graphene coverage. (Figure 4.2a)[41] By comparing the depths and shapes, we were able to clearly distinguish between the suspended graphene and the empty holes. The suspended graphene exhibited a sag of approximately 50 nm (illustrated by the black line in Figure 4.2b)[41], whereas the shape depicted by the red line corresponds to the convolution of the hole with the AFM tip. This shape aligns with prior research utilizing tapping mode in the AFM system.[42]

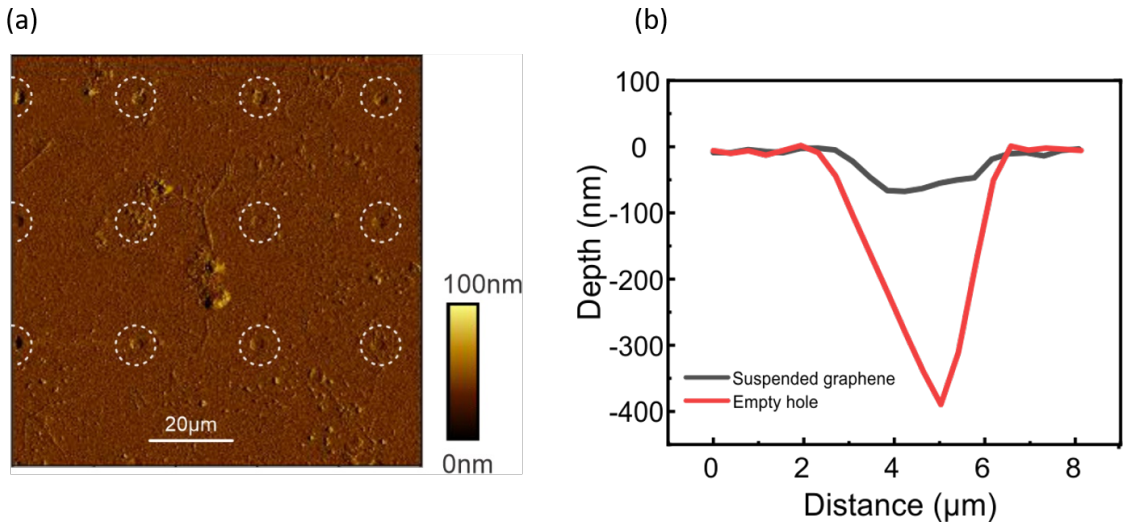

Figure 4.2: (a) AFM mapping illustrates the coverage of suspended graphene, while (b) depicts the depth of suspended graphene and vacant holes on the substrate.

SEM imaging reveals that the cobalt electrodes have perfectly enclosed the suspended graphene, as depicted in the high-resolution visualized image. (Figure 4.3)[41] In order to compare UCD-GSVs and c-GSVs, we conducted a cross-sectional SEM analysis to assess the quality of the interface. Cobalt is susceptible to oxidation in ambient conditions, but the limited diffusivity of oxygen leads to a constrained oxide thickness.[43] This phenomenon is evident in cross-sectional SEM images of conventional c-GSVs, where a distinct color contrast is observed in the ferromagnetic electrodes near the graphene layer. (Figure 4.4a)[41] This contrast indicates that the bottom-Co contact is not in direct contact

doi:10.6342/NTU202400068

with graphene but is separated by an oxide layer. Additionally, empty regions between the graphene and the bottom electrode are visible, formed when the graphene was suspended over imperfections in the bottom electrode.

In contrast, our UCD-GSVs show no signs of an oxide layer between the graphene and Co, as evidenced by a uniform contrast in the cross-sectional image. (Figure 4.4b)[41] Furthermore, close examination reveals the absence of empty regions between the ferromagnetic contacts, confirming the conformal deposition. This observation is further supported by EDX analysis, which demonstrates the absence of any oxygen elements within the interface. (Figure 4.5)[41]

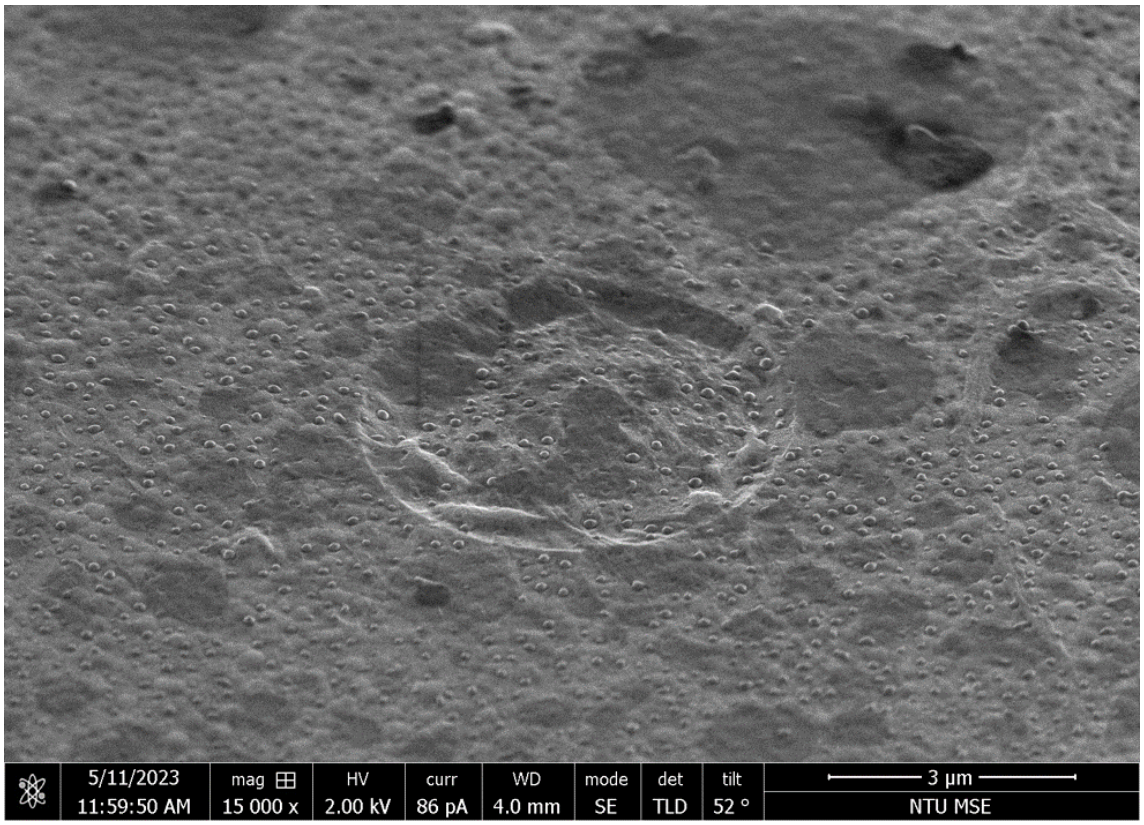

Figure 4.3: SEM image explains the Co deposition fully covers the suspended graphene.

doi:10.6342/NTU202400068

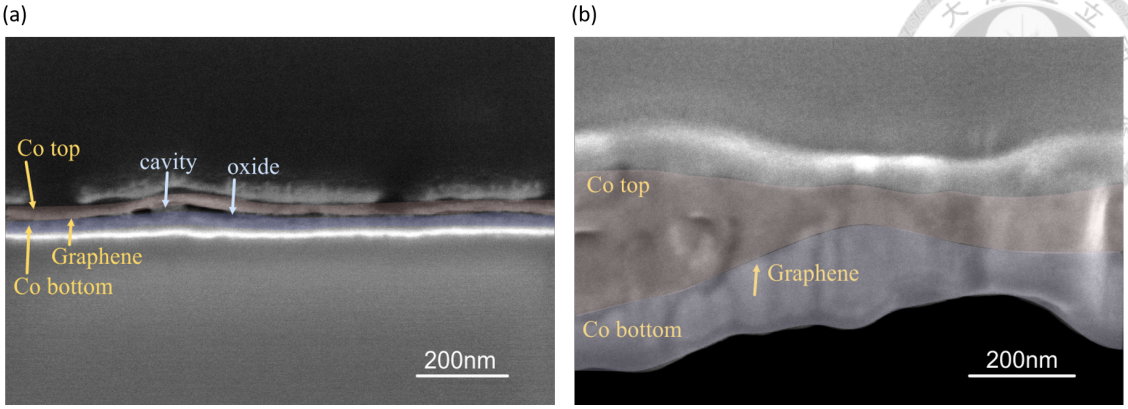

Figure 4.4: (a) cross-sectional SEM of c-GSVs, and (b) UCD-GSVs.

4.1.2 Analysis of electric property

The tightness of the layers significantly impacts the conductivity of the components. Figure 4.6[41] illustrates the geometry of electric measurement. Electrical properties were investigated through the relationship between voltage and current. UCD-GSVs exhibit a current density magnitude four orders of magnitude higher than c-GSVs at 300K. (Figure 4.7)[41]

To comprehend the origin of this enhancement, we employed ab-initio calculations to simulate the interface conditions in UCD-GSVs and c-GSVs. Two ferromagnetic contacts were positioned on each side of a graphene layer, and the resulting band structure was calculated using density functional theory (DFT). In the case of UCD-GSVs, two cobalt cells were separated by a graphene layer, while for c-GSVs, partial oxidation was introduced at one interface.

In UCD-GSVs, a strong hybridization was observed, causing a significant change in graphene's density of states around the K-point, where carrier transport is anticipated. This effect indicates a robust interaction between graphene and the contact, elucidating the high interfacial conductivity (Figure 4.8a)[41]. Conversely, oxidation in c-GSVs alters the

doi:10.6342/NTU202400068

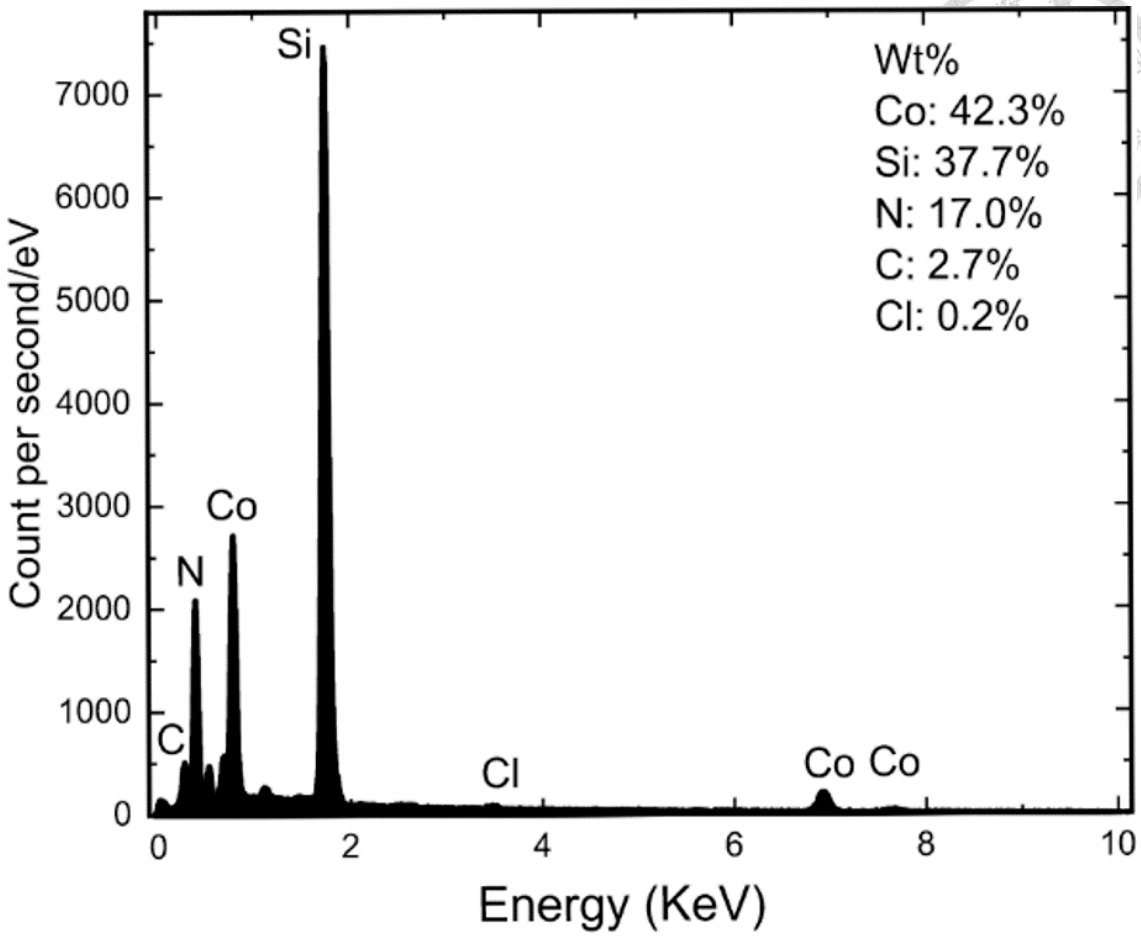

Figure 4.5: Element analysis in the interface of UCD-GSVs using EDX.

interface band structure, and a reduced density of states at the K-point suggests a weaker interaction between cobalt and graphene, resulting in higher interfacial resistance (Figure 4.8b)[41].

4.1.3 Magnetotransport in UCD-GSVs

Magneto-transport experiments were conducted for both interface types, namely conventional and clean surfaces. An in-plane magnetic field, aligned with the easy-axis of the Co thin film, was applied to both the UCD-GSVs and c-GSVs to observe the MR phenomenon (Figure 4.9)[41]. The Figure 4.10[41] illustrates the difference in resistance as the magnetic field is swept. Notably, c-GSVs did not exhibit any discernible MR within

doi:10.6342/NTU202400068

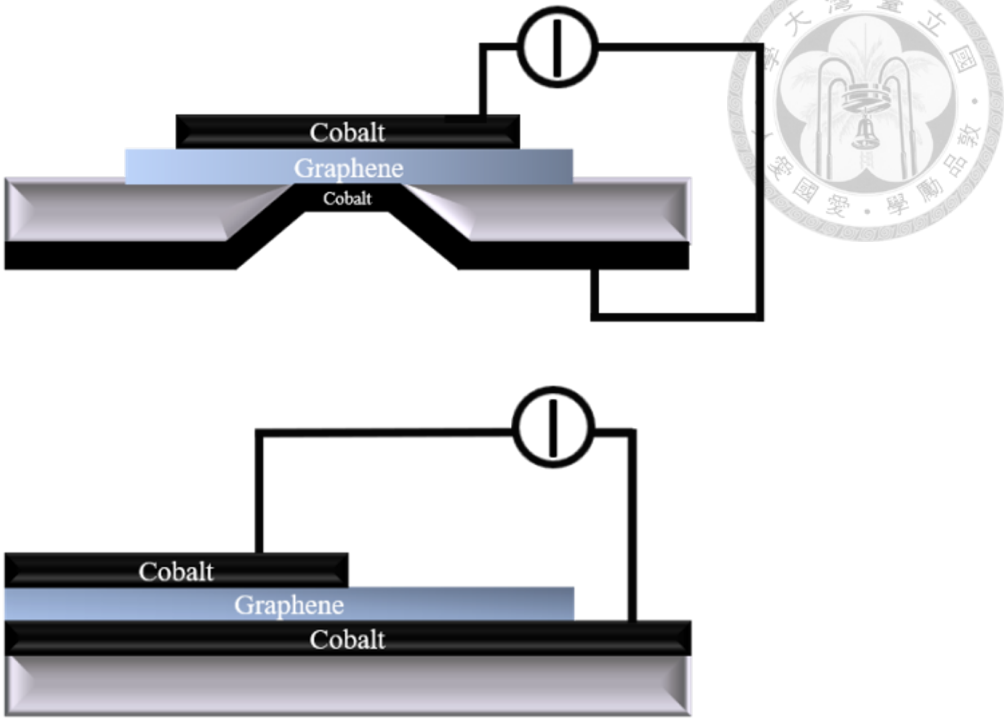

Figure 4.6: Geometries for IV measurements of UCD-GSVs and c-GSVs.

the resolution of our experiments. In contrast, the measured MR (MR) in UCD-GSVs reached a value of 1.7%, surpassing those reported in previous studies on graphene-based spin valves [19, 20, 29, 44], (refer to Table4.1 for a comparison with other research findings).

Structure	MR (%)	Temp (K)	Reference
Co/Gr/Co	0.7	1.5	Meng, J. (2013)
Co/Gr/Co	0.7	3	Chen, J.-J (2013)
Co/Gr/NiFe	0.23	10	Iqbal (2015)
Co/Gr/NiFe	0.1	10	Asshoff, P. (2017)
Co/Gr/Co	1.7	10	our work

Table 4.1: MR comparison in Co/Gr/Co spin valves

To further experimentally assess the quality of the spin-valve interfaces, we changed the magnetic field direction from in-plane to out-of-plane. This perpendicular alignment to the easy-axis enhances the spin precession of electrons at the interface between the barrier and ferromagnetic contact. The resulting relaxation of injection conditions leads to the

doi:10.6342/NTU202400068

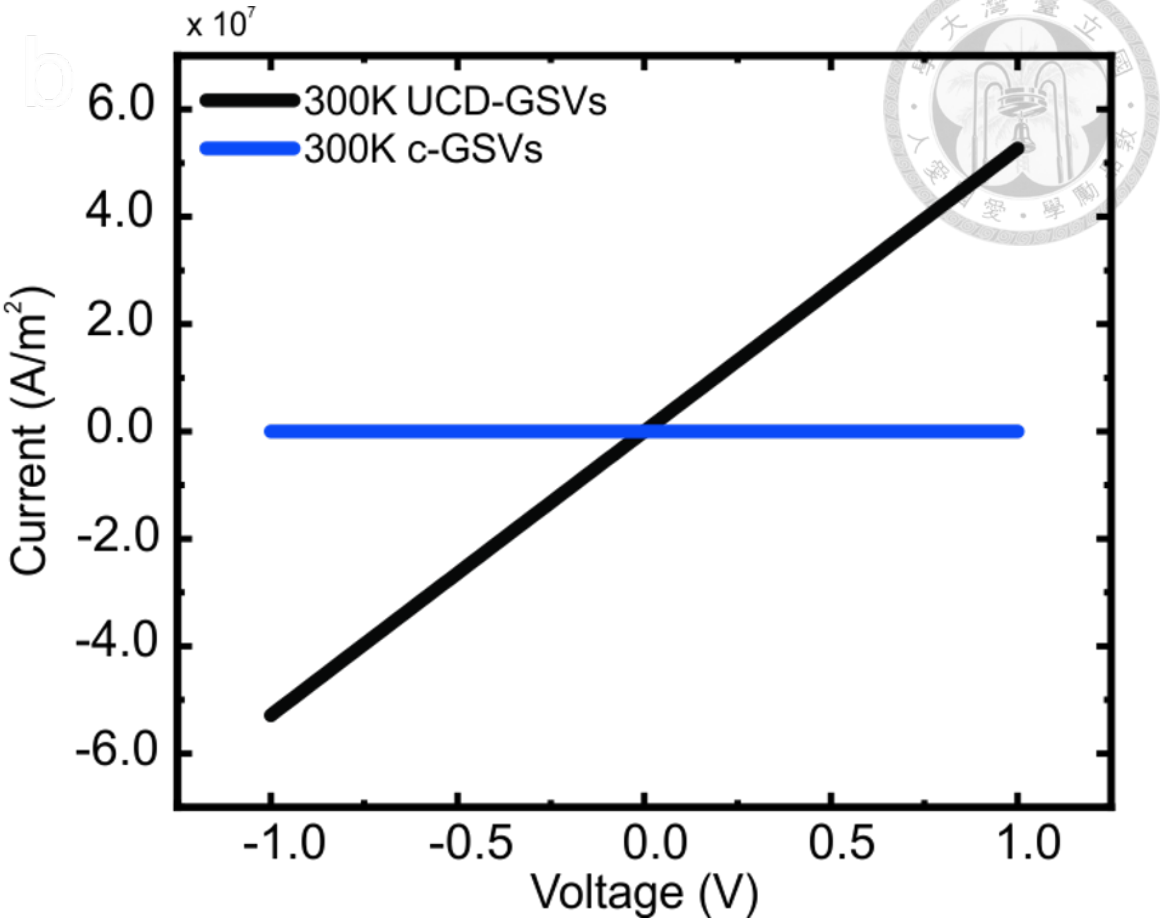

Figure 4.7: IV curves comparison at 300 K.

well-known Hanle effect[45], which decreases the MR (MR) value with an increasing magnetic field.

A comparison of the voltage difference between c-GSVs and UCD-GSVs reveals a significantly smaller voltage change in the zero-field value for UCD-GSVs (Figure 4.11).[41] This behavior indicates a lesser accumulation of spin-polarization at the high-quality interface[45, 46]. With the substantial difference in interface quality confirmed, we can employ the comparison between UCD-GSVs and c-GSVs to establish the limitations of using the Hanle effect for the characterization of electron spins.

Following this approach, the spin lifetime (t) of c-GSVs is twice as long as UCD-GSVs (0.227 ns vs. 0.117 ns) and higher than in previous reports.[47] This observation

doi:10.6342/NTU202400068

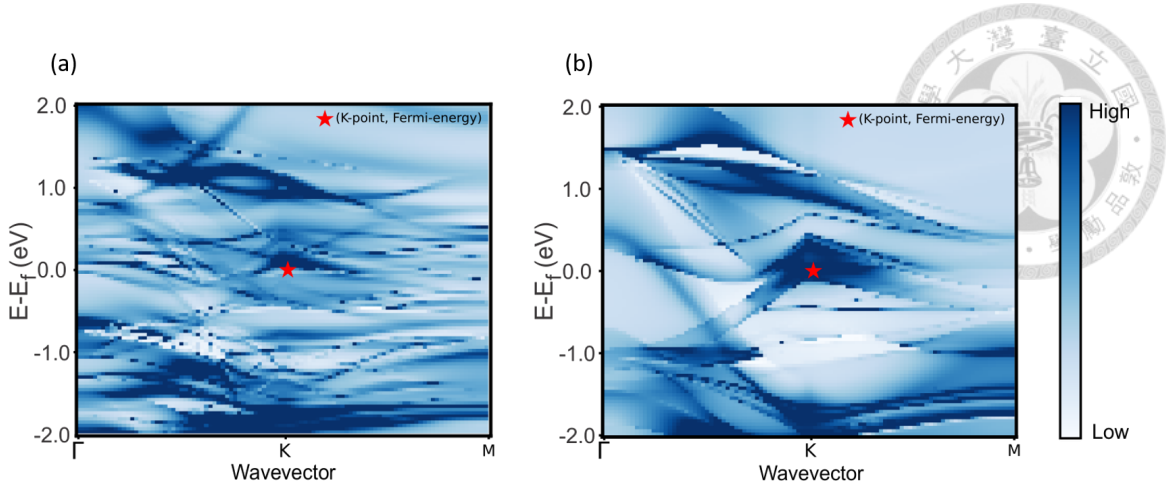

Figure 4.8: (a) interface band structure of CoO/graphene/Co, and (b) interface band structure of Co/graphene/Co.

underscores the impact of back-scattering from low-quality interfaces on spin accumulation [47]. Our results demonstrate that the formation of high-quality interfaces enables the study of the intrinsic magnetic response of 2D materials.

The investigation into the properties of suspended graphene involves diverse analytical techniques. Raman spectroscopy provides insights into the graphene's continuity, revealing a downshifted G-band feature in the suspended region, indicating the relaxation of tensile strain. AFM mapping and SEM imaging further confirm structural integrity, emphasizing the effectiveness of graphene transfer methods. UCD-GSVs demonstrate superior interface quality, impacting electron spin behavior. Magnetotransport experiments highlight significant MR differences, and the Hanle effect reveals limitations in characterizing electron spins. These findings emphasize the importance of high-quality interfaces for studying 2D materials' intrinsic magnetic responses.

4.1.4 Multilayer graphene spin valves

We employ the UCD approach in the context of multi-layer graphene spin valves (UCD-mGSVs) due to their potential applications in spintronics[47]and twisttronics [48].

doi:10.6342/NTU202400068

In contrast to single-layer graphene, UCD-mGSVs exhibit a non-linear current-voltage relationship indicative of tunneling-dominated carrier transport[27] (Figure 4.12). This effect arises from the presence of a non-zero bandgap in multilayer graphene, introducing a barrier absent in single-layer graphene.[49]

The impact of this barrier on spin injection becomes apparent when characterizing the Hanle effect in UCD-mGSVs (Figure 4.13). The higher spin concentration leads to increased scattering and a greater loss of spin information, resulting in shorter spin relaxation times.[50] Indeed, we observe a 26% decrease in carrier lifetime compared to UCD-GSVs. Moreover, there is a 70% decrease in the MR (MR) change, confirming the lower tunneling rate through the multilayer and the associated increase in spin accumulation at the interfaces (Figure 4.14).

This interplay between spin transport and spin scattering is typically not considered theoretically when predicting the performance of GSVs, potentially leading to an overestimation of achievable MR. Our findings reveal that the MR for multilayer GSVs is less than that for single-layer GSVs.

doi:10.6342/NTU202400068

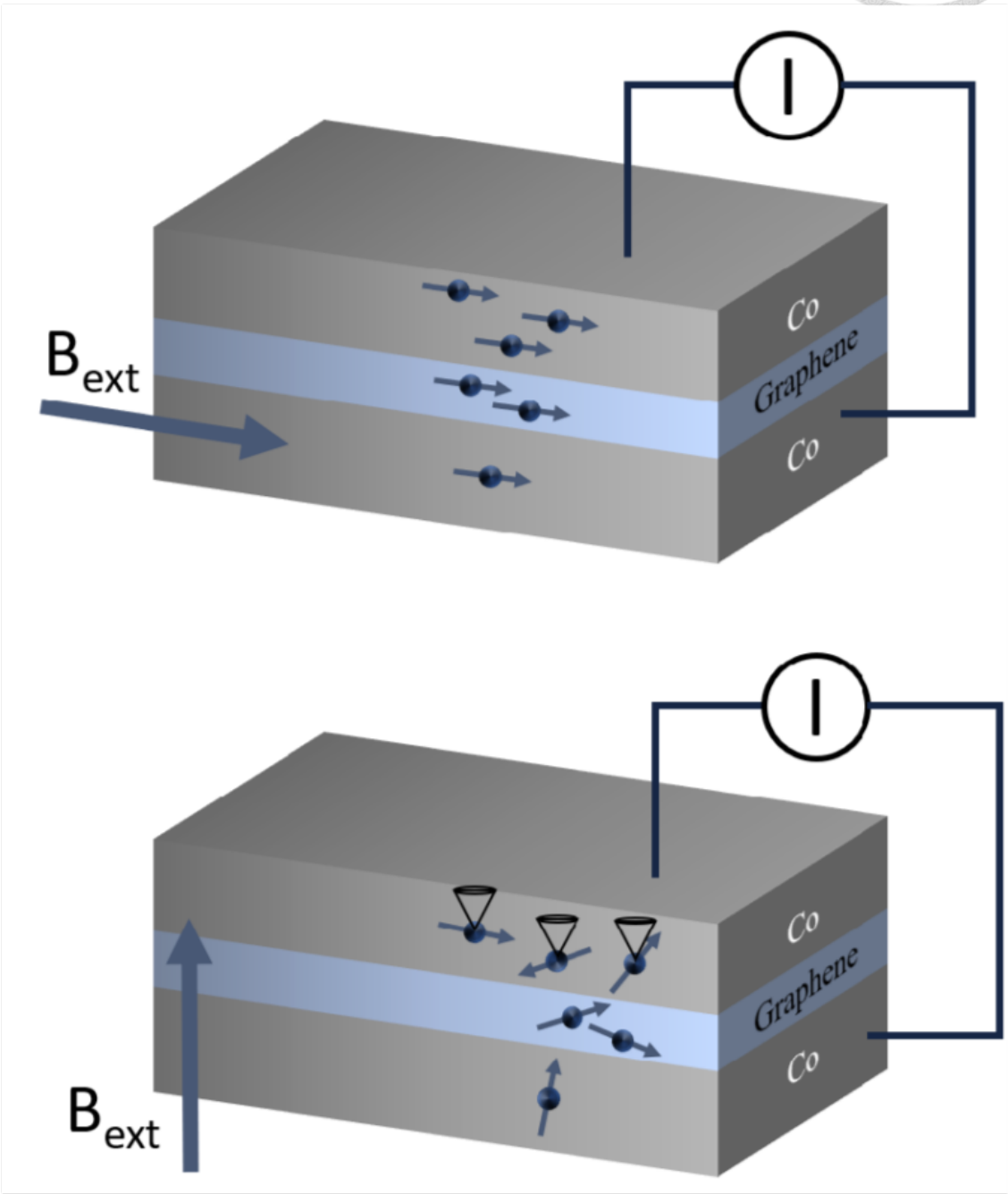

Figure 4.9: Geometries for MR measurement with in-plane or out-plane external magnetic field.

doi:10.6342/NTU202400068

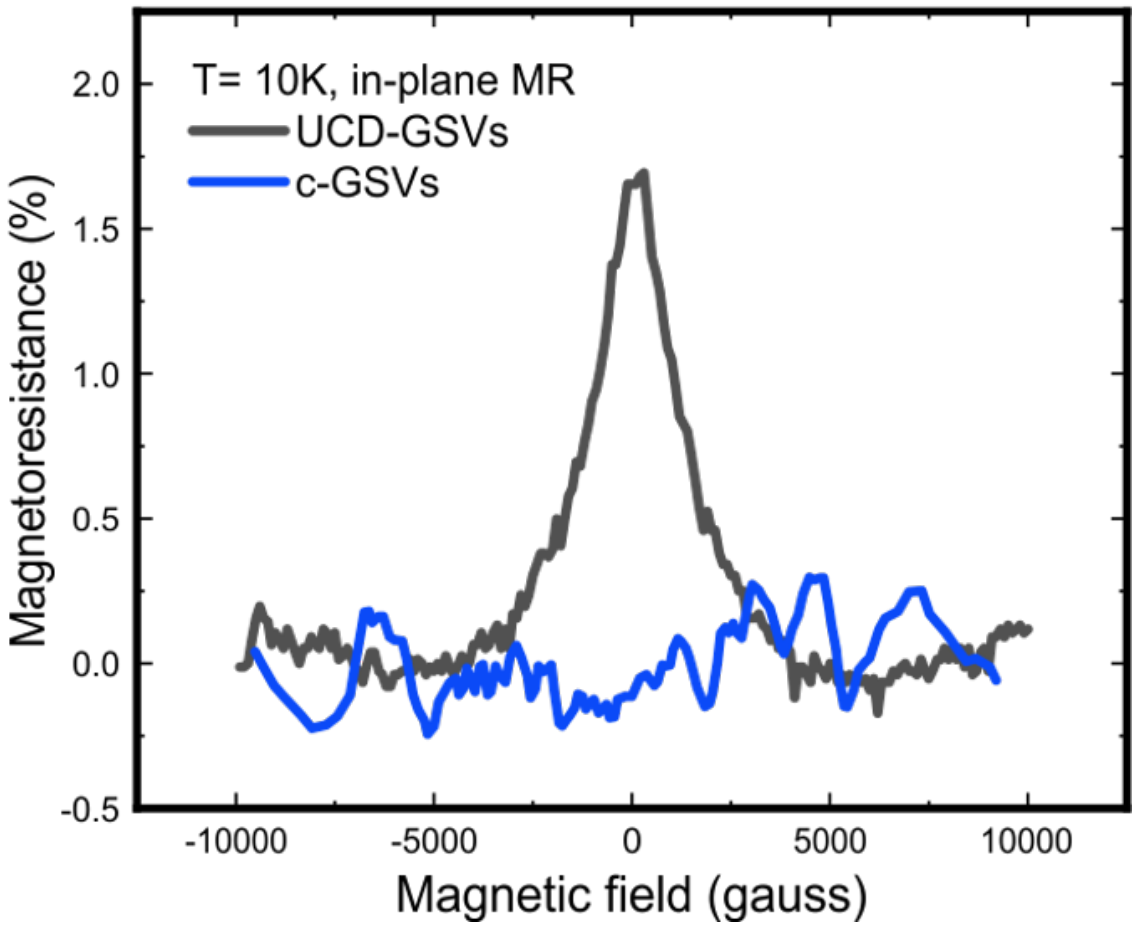

Figure 4.10: In-plane MR analysis of UCD-GSVs and c-GSVs.

doi:10.6342/NTU202400068

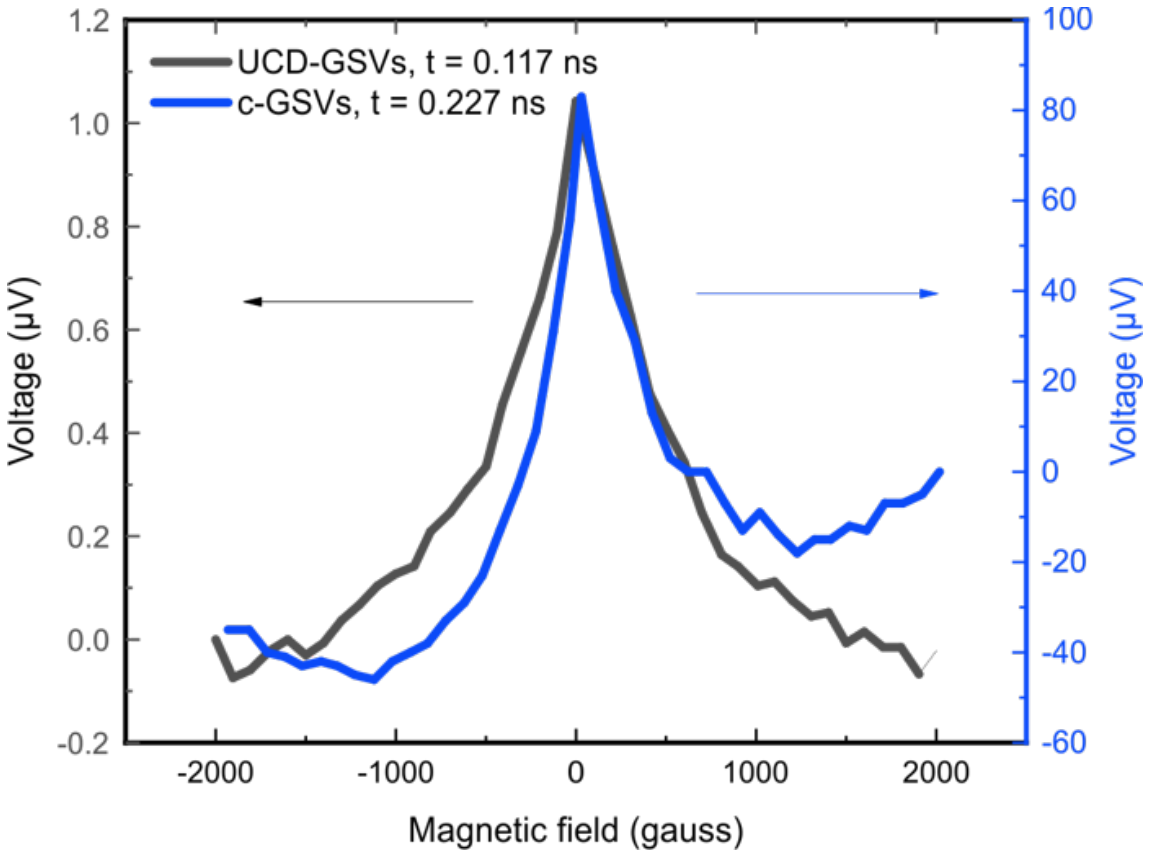

Figure 4.11: Out-plane MR analysis of UCD-GSVs and c-GSVs.

doi:10.6342/NTU202400068

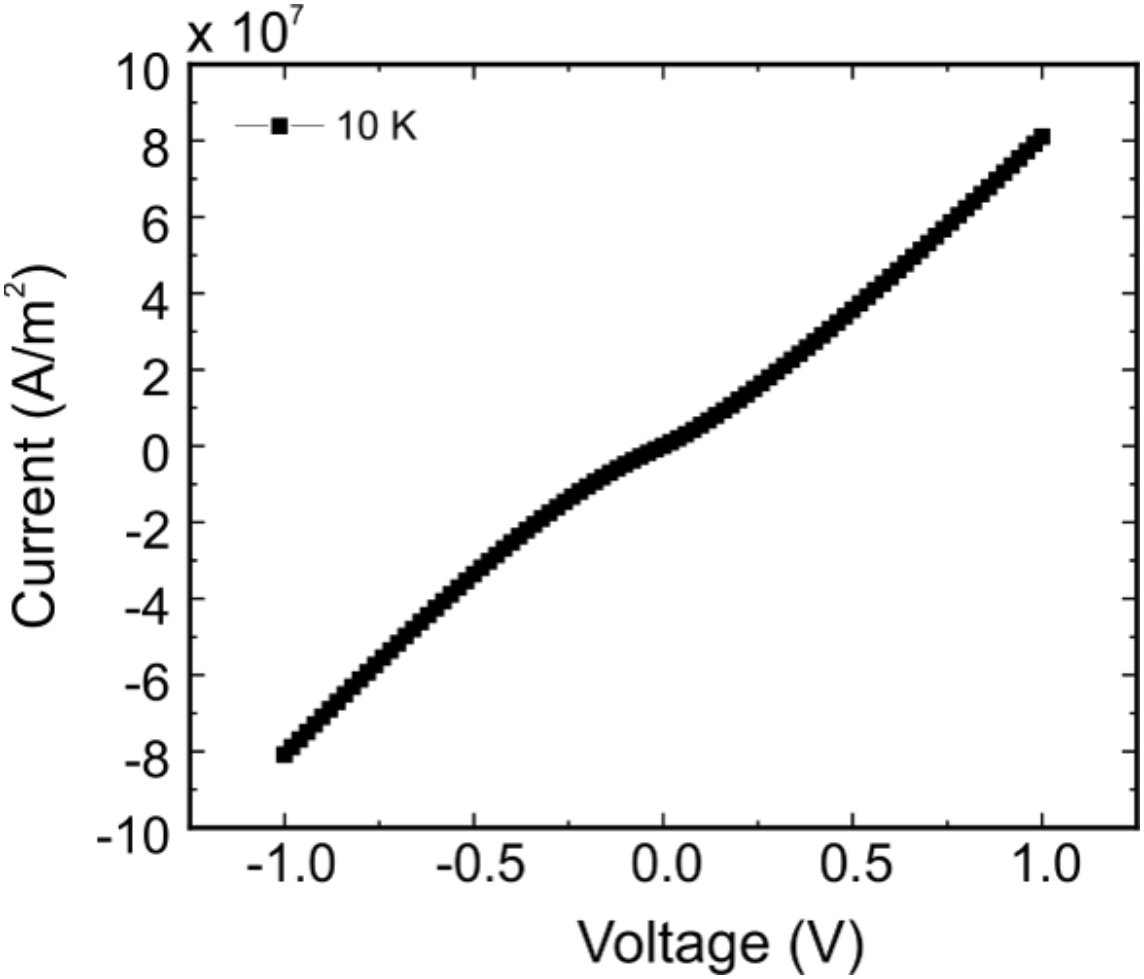

Figure 4.12: Non-linear IV curve in UCD-mGSVs.

doi:10.6342/NTU202400068

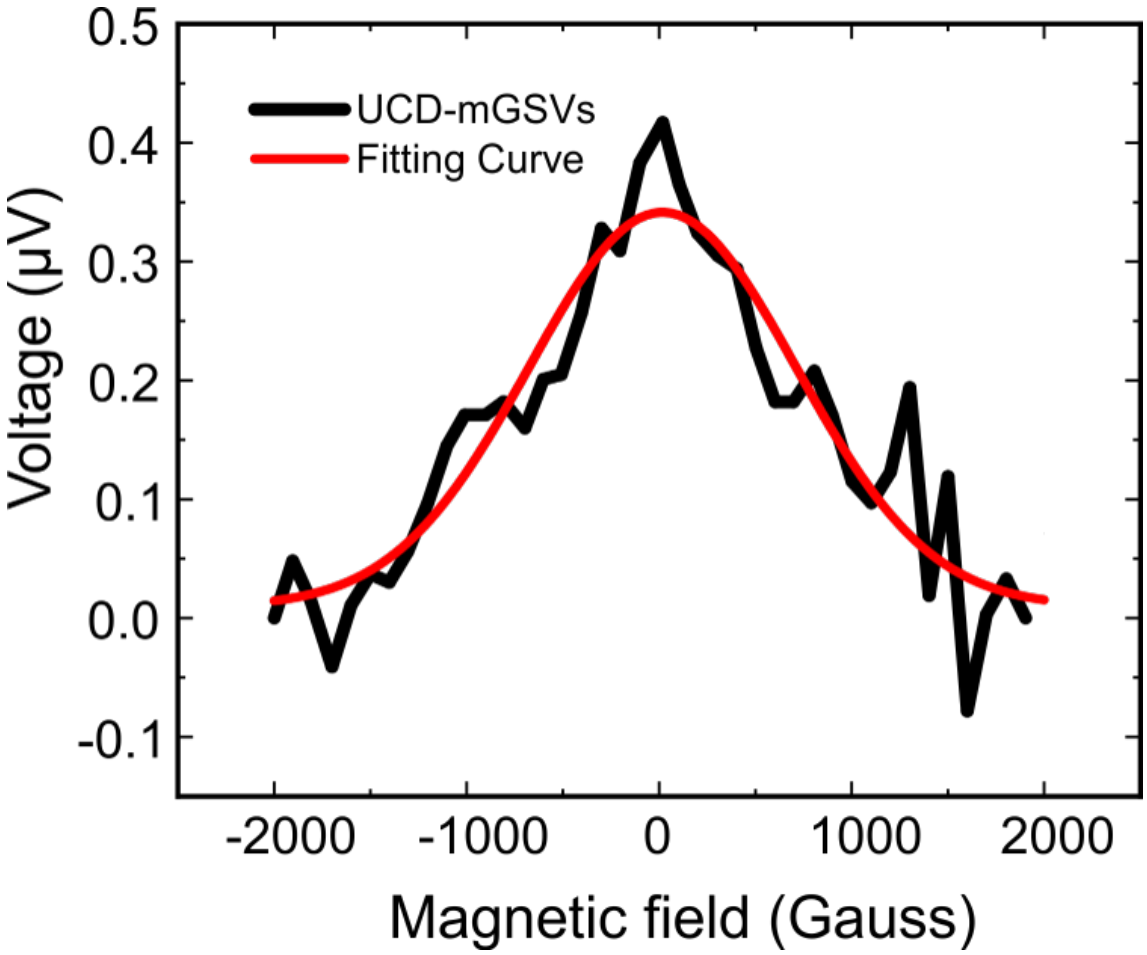

Figure 4.13: Hanle measurement and analysis in UCD-mGSVs.

doi:10.6342/NTU202400068

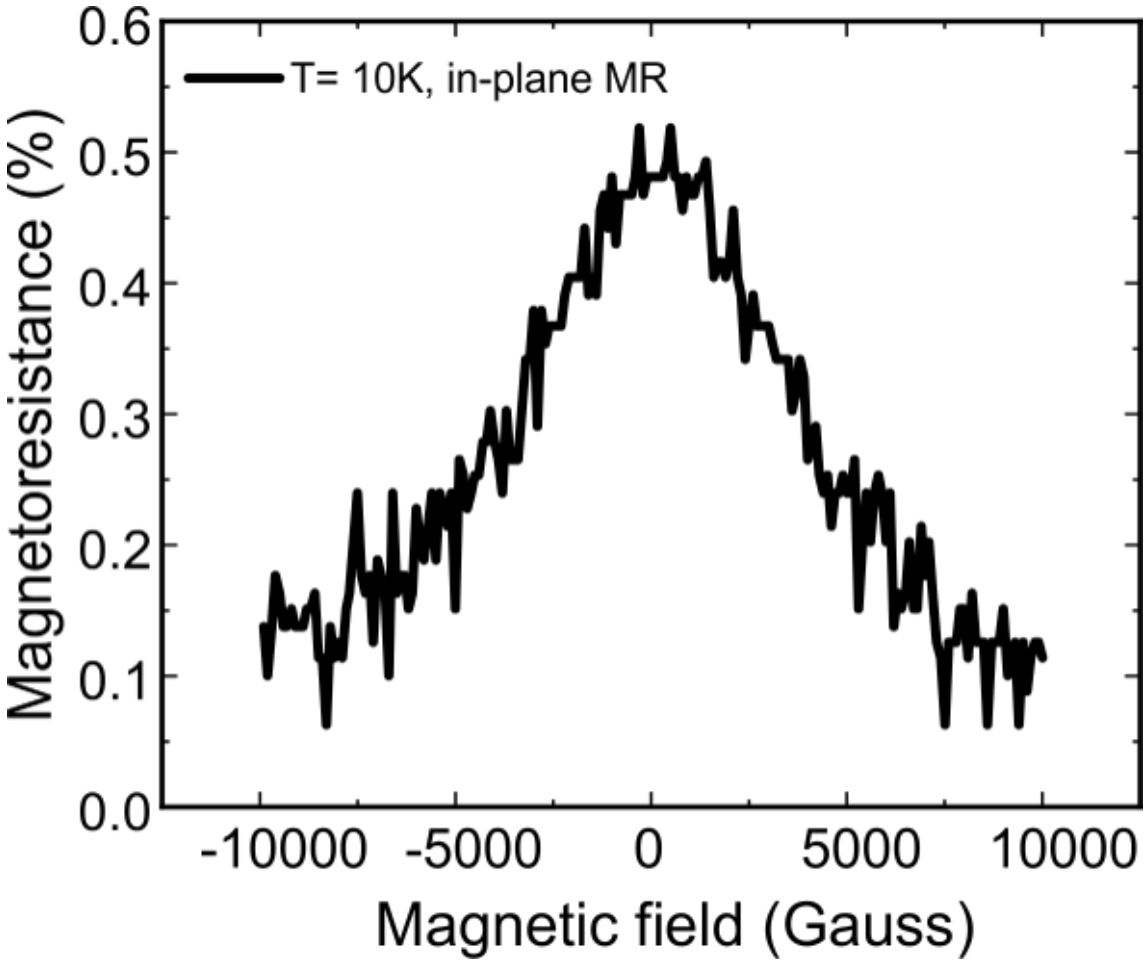

Figure 4.14: In-plane MR analysis of UCD-mGSVs.

doi:10.6342/NTU202400068

4.2 Controllable Coercivity in NiFe-Graphene Spin Valves

Permalloy (NiFe), a ferromagnetic alloy composed of 20% iron and 80% nickel, possesses high magnetic permeability, low coercivity, and pronounced magnetic anisotropy. These characteristics make NiFe a promising candidate for spin valves with controllable coercivity. Therefore, we employed the UCD method in an attempt to engineer spin valves with nearly zero coercivity characteristics in NiFe.

4.2.1 Investigating the electrical properties of NiFe-GSVs

Controllable coercivity spin valves, denoted as NiFe-GSVs, comprise a structure of NiFe/graphene/NiFe. The linear current-voltage relationship depicted in Figure 4.15 illustrates Ohmic contact within this configuration, indicating intimate contact at the NiFe-graphene interface. In contrast to metallic behavior, the temperature-dependent resistance reveals semiconductor characteristics, manifesting increased resistance with decreasing temperature (Figure 4.16). This electric performance explains why the graphene spacer dominates the electronic transport in the NiFe-GSVs.

4.2.2 Magnetotransport in NiFe-GSVs

External magnetic fields, either parallel or perpendicular, are applied to investigate the magnetic response of NiFe-GSVs. In the parallel configuration, the MR prominently centers around zero magnetic field, confirming the intrinsic coercivity of our NiFe-GSVs —an original component for crafting controllable spin valves. Furthermore, at 10 K, the MR variation reaches 1.3%, surpassing previous findings by adjusting asymmetric spin

doi:10.6342/NTU202400068

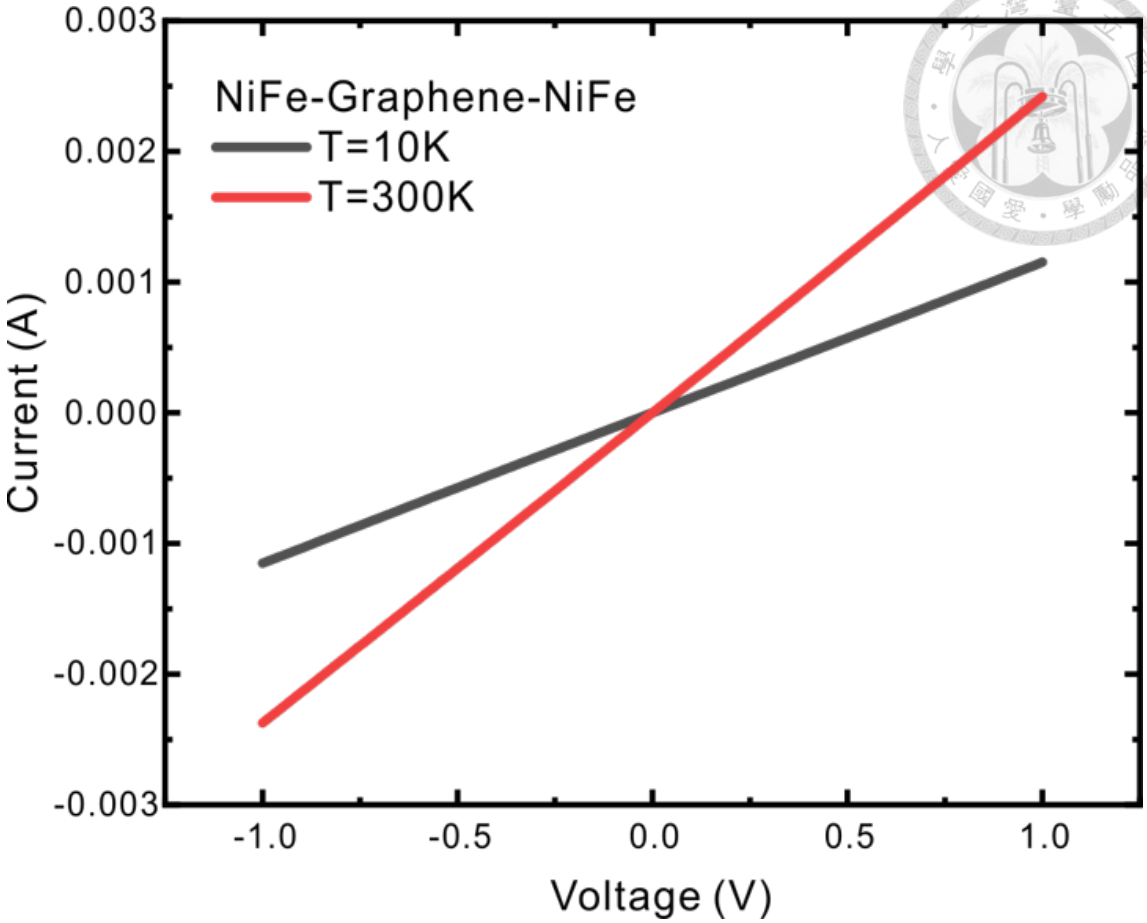

Figure 4.15: Temperature-dependent IV curves in NiFe-GSVs

quantities in both electrodes (Figure 4.17). Similarly, in the case of an externally perpendicular magnetic field, the MR feature is also centered at zero field, indicating the low coercivity properties of NiFe. However, owing to the magnetic anisotropy of NiFe, the magnetic resistance variation in this direction is more pronounced than in the parallel orientation (Figure 4.18). The MR decreases with increasing temperature due to thermal disturbances.[51]

4.2.3 Controllable coercivity in NiO-NiFe-GSVs

The geometry for electric and magnetic transport measurements is illustrated in the Figure 4.19. The magnetization curve shift is a significant phenomenon observed when a ferromagnet interfaces with an antiferromagnet[50, 52]. NiO, a typical antiferromagnetic

doi:10.6342/NTU202400068

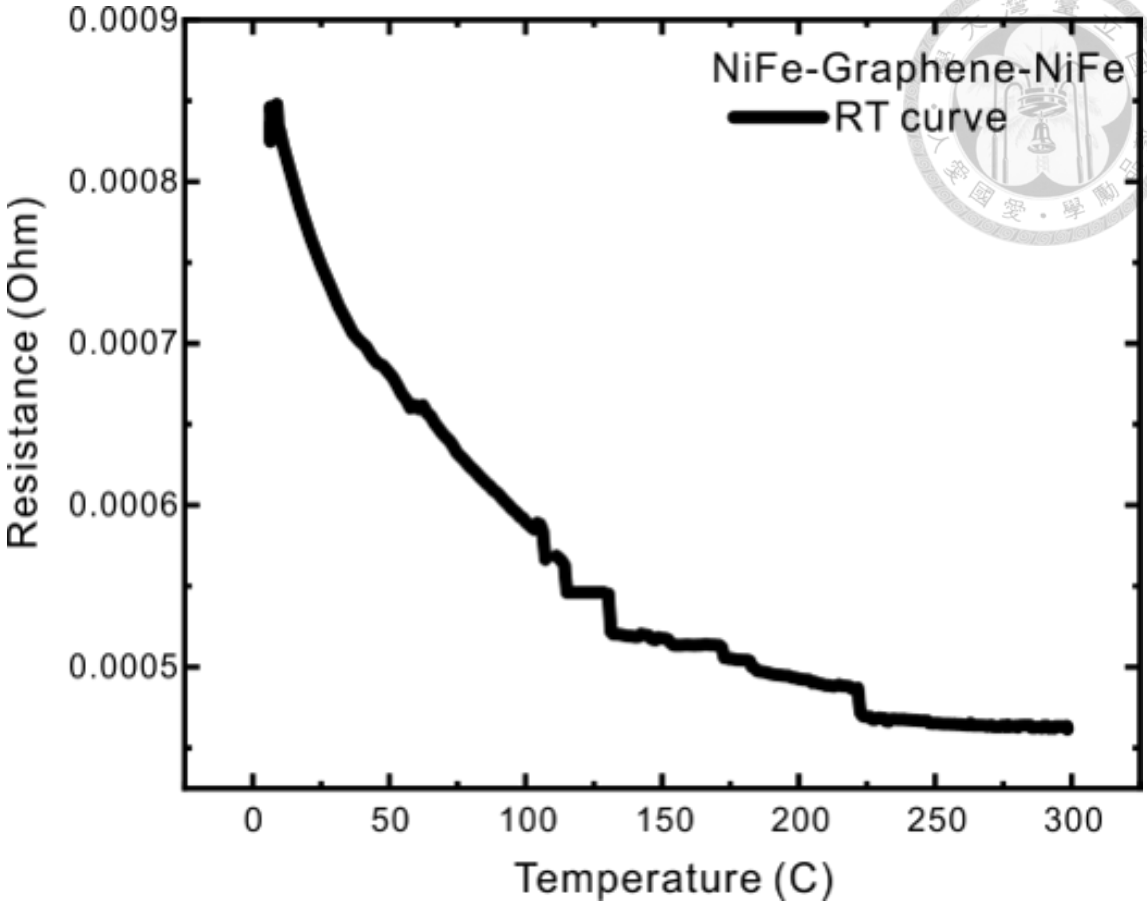

Figure 4.16: Resistance and temperature relationship of NiFe-GSVs.

insulator, exhibits strong interactivity with NiFe owing to the exchange bias effect.[50] Consequently, we incorporated NiO on either side of NiFe-GSVs to attain controllable coercivity. We refer to this device as NiO-NiFe-GSVs.

In the relationship between current and voltage (Figure 4.20), we did not observe significant variations in the conductivity of NiO-NiFe-GSVs compared to NiFe-GSVs, despite the insulating nature of NiO. This finding highlights the potential utility of NiO in electronic devices, where it can provide insulation to prevent current leakage and exhibit protective characteristics due to its highly corrosion-resistant properties without compromising electrical performance.[53]

NiO, serving as the pinned layer in the spin valve, induces a more asymmetrical distribution of spin quantities when the direction of the external magnetic field is switched.

doi:10.6342/NTU202400068

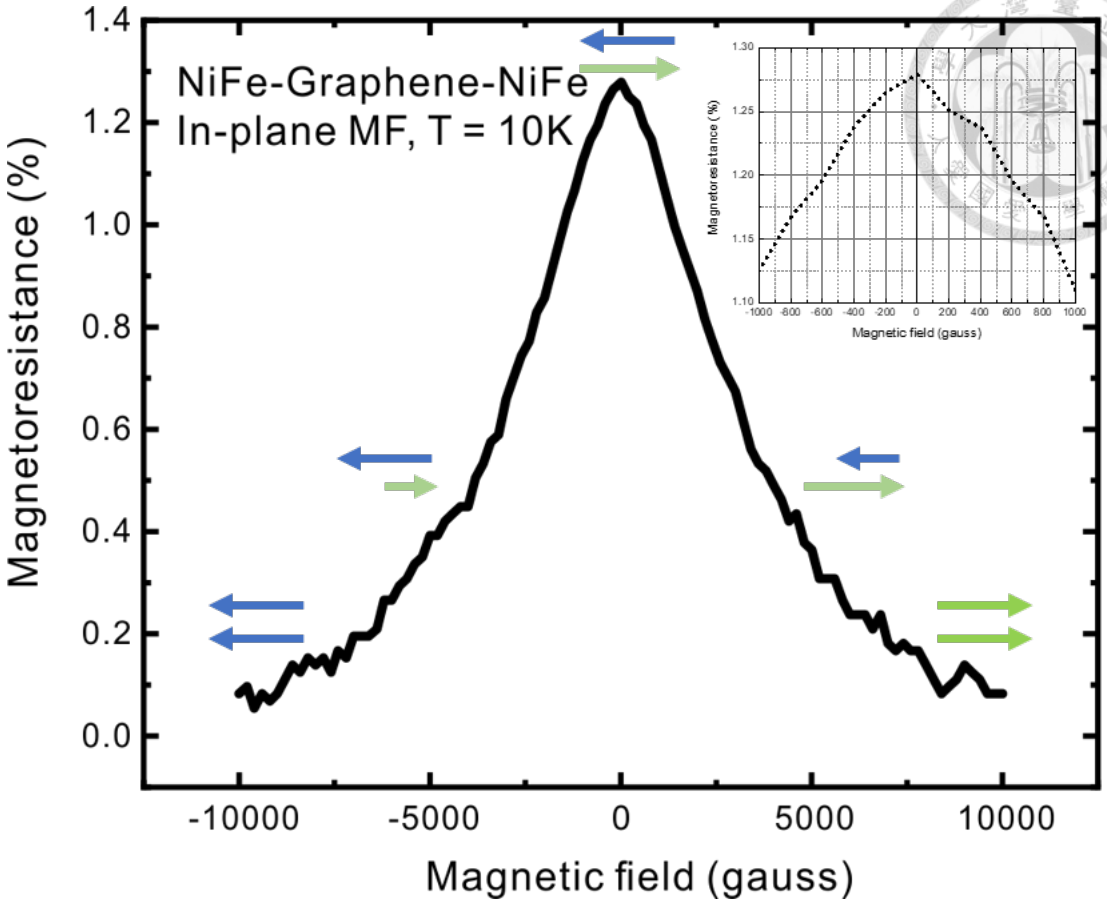

Figure 4.17: In-plane MR analysis of NiFe-GSVs; Inset: magnified MR plot in the vicinity of zero magnetic field.

Consequently, the MR variation is significantly enhanced to 2.8% in NiO-NiFe-GSVs under an in-plane external magnetic field (Figure 4.21), which is twice that observed in NiFe-GSVs. Additionally, NiO-NiFe-GSVs still present an inverse relationship between temperature and resistance, showing semiconductor behavior induced by graphene is dominant in this system. In Table 4.2, we compare the magnetoresistance (MR) results from our structure with those of a similar spin valve configuration.

A similarly enhanced magnitude of MR is observed in the perpendicular magnetic field situation (Figure 4.22). Simultaneously, NiO-NiFe-GSVs still exhibit anisotropy, with a more pronounced feature in a small range of magnetic fields.

Particularly noteworthy is the distinct shift observed in the MR characteristics of

doi:10.6342/NTU202400068

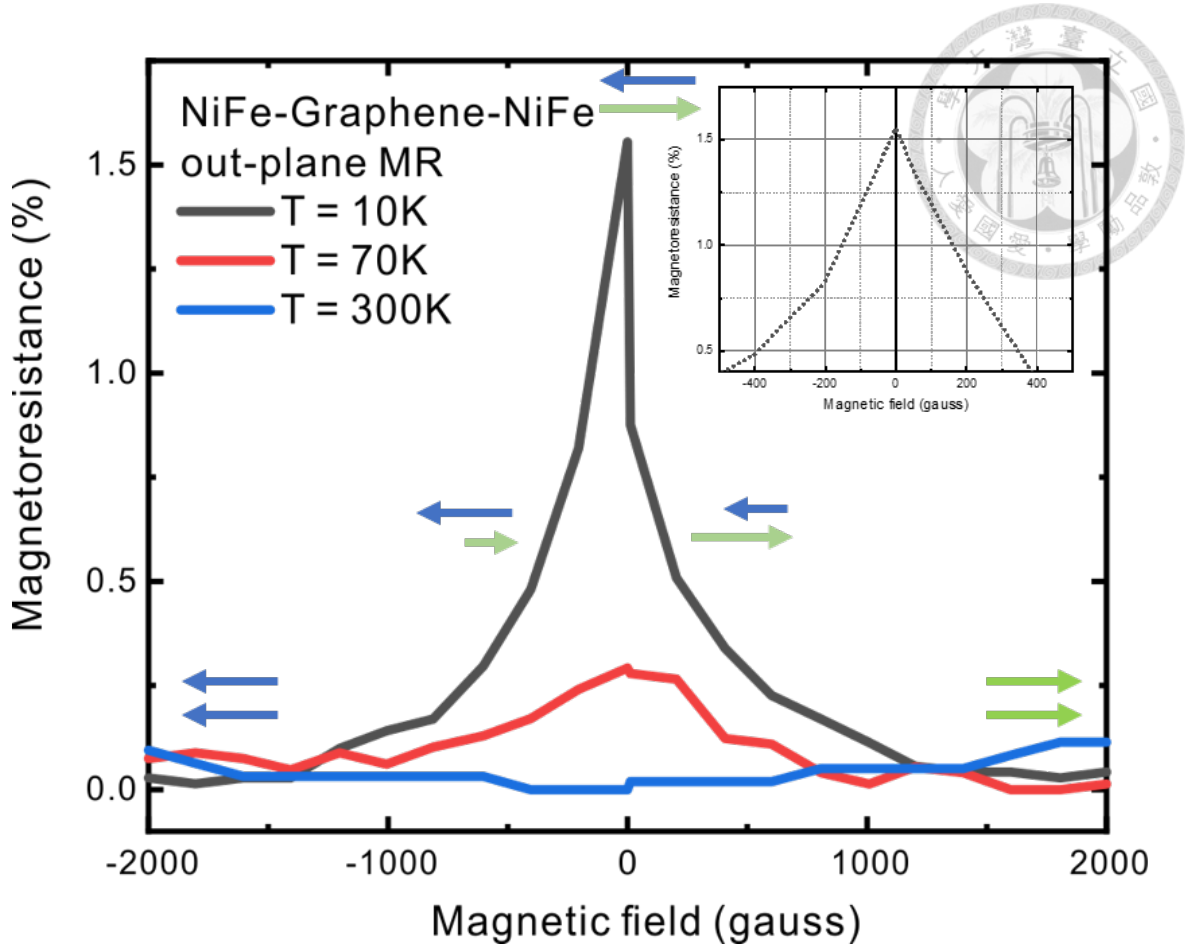

Figure 4.18: Out-plane MR analysis of NiFe-GSVs; Inset: magnified MR plot in the vicinity of zero magnetic field.

NiO-NiFe-GSVs during scans in different directions (see Figure 4.2.8). When the external magnetic field aligns parallel to the direction of electron travel, it induces anisotropic MR (AMR), causing the MR to increase with the magnetic field. In large magnetic fields, we precisely determine the displacement caused by coercivity through the generated differences in MR. (Figure 4.23) During scans in different directions, the MR curves exhibit a gap of 514.7 gauss, indicating that the Exchange bias between NiO and NiFe elevates the originally nearly zero coercivity by approximately 207 gauss. This difference corresponds to previous reports on NiO/NiFe.[8, 52] Our result signifies the successful fabrication of a controllable coercivity spin device, offering richer applications for spin valves through the manipulation of coercivity.

doi:10.6342/NTU202400068

Spin transport behavior can be studied by examining the relaxation of spin accumulation at the interface. Analyzing the voltage changes with magnetic field variations provides information on the spin lifetime in the systems.[33] NiFe-GSVs and NiO-NiFe-GSVs exhibit spin lifetimes of 0.213 ns and 0.154 ns, respectively (Figure 4.24). The shorter spin lifetime in the NiO-NiFe-GSVs is attributed to oxygen vacancies present in the oxides, which act as traps for the spin.[50]The vacancy features are evident around 401 cm^{-1} shift[54] in our Raman spectroscopic results on NiO (Figure 4.25).

Structure	MR (%)	Method	Reference
NiFe/Gr/NiFe	0.4	Exfoliation	Mohiuddin *et al* (2008)
NiFe/Gr/NiFe	0.14	Wet transfer	Iqbal *et al* (2013)
NiFe/Gr/NiFe	0.29	Direct CVD on FM	Entani *et al* (2016)
NiFe/Gr/NiFe	1.3	UCD	Our work
NiO/NiFe/Gr/NiFe	2.7	UCD	Our work

Table 4.2: MR comparison in NiFe/Gr/NiFe spin valves

To conclude, NiFe essentially exhibits its intrinsic response with near-zero coercivity in the spin valve when subjected to a magnetic field using our UCD method. Furthermore, we successfully manipulated the coercivity in the spin valve by incorporating NiO on one side. Additionally, NiO significantly enhanced the MR without compromising the conductivity performance.

doi:10.6342/NTU202400068

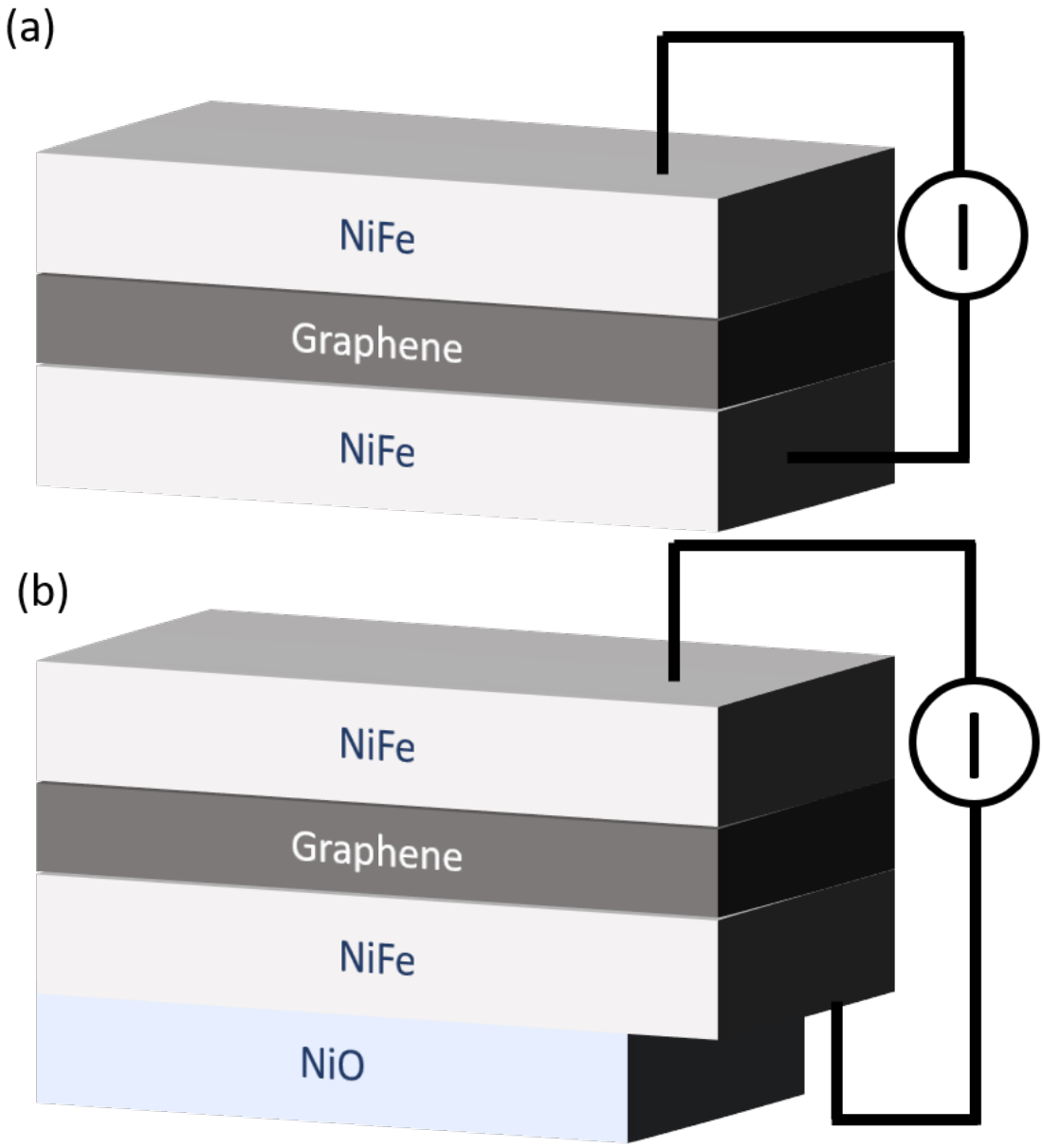

Figure 4.19: Geometries for electric and magnetic measurement for (a) NiFe-GSVs and (b) NiO-NiFe-GSVs.

doi:10.6342/NTU202400068

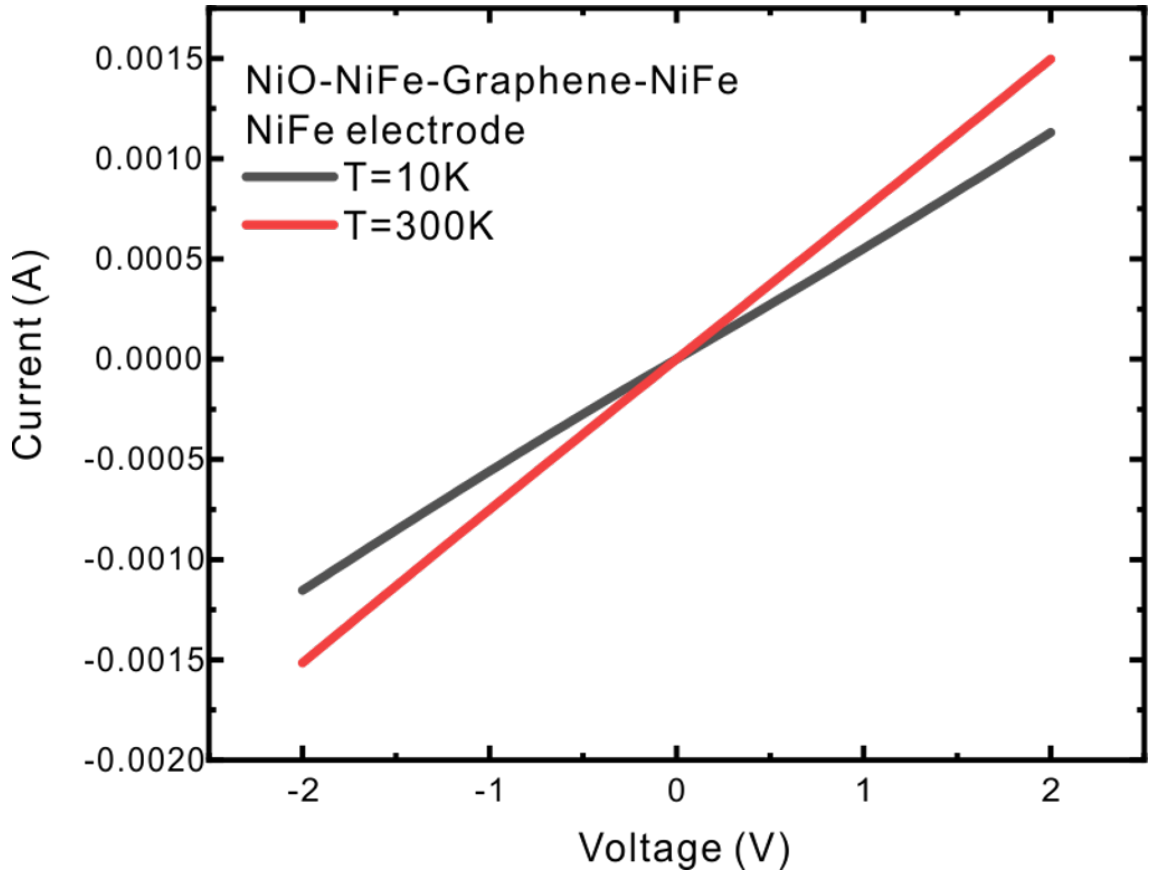

Figure 4.20: Temperature-dependent IV measurement for NiO-NiFe-GSVs.

doi:10.6342/NTU202400068

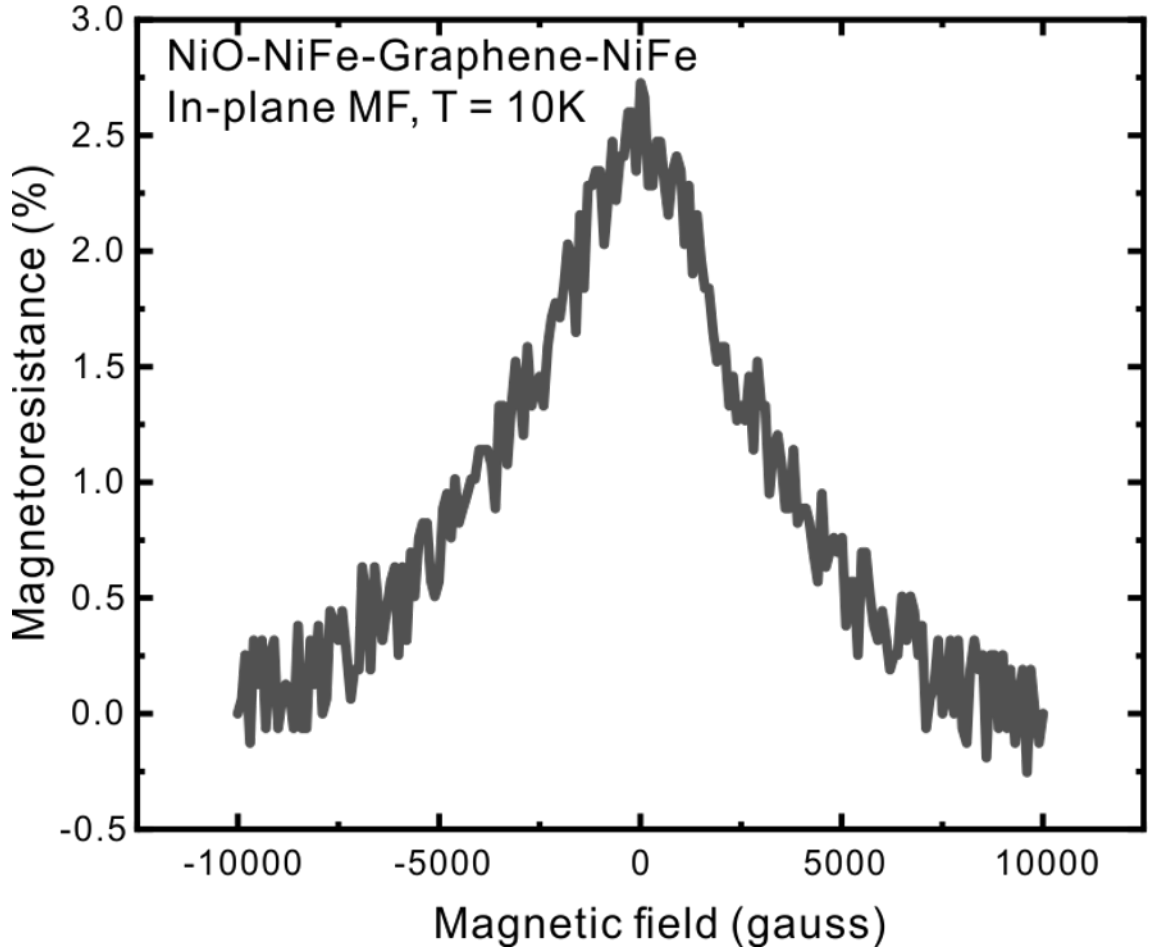

Figure 4.21: In-plane MR analysis of NiO-NiFe-GSVs.

doi:10.6342/NTU202400068

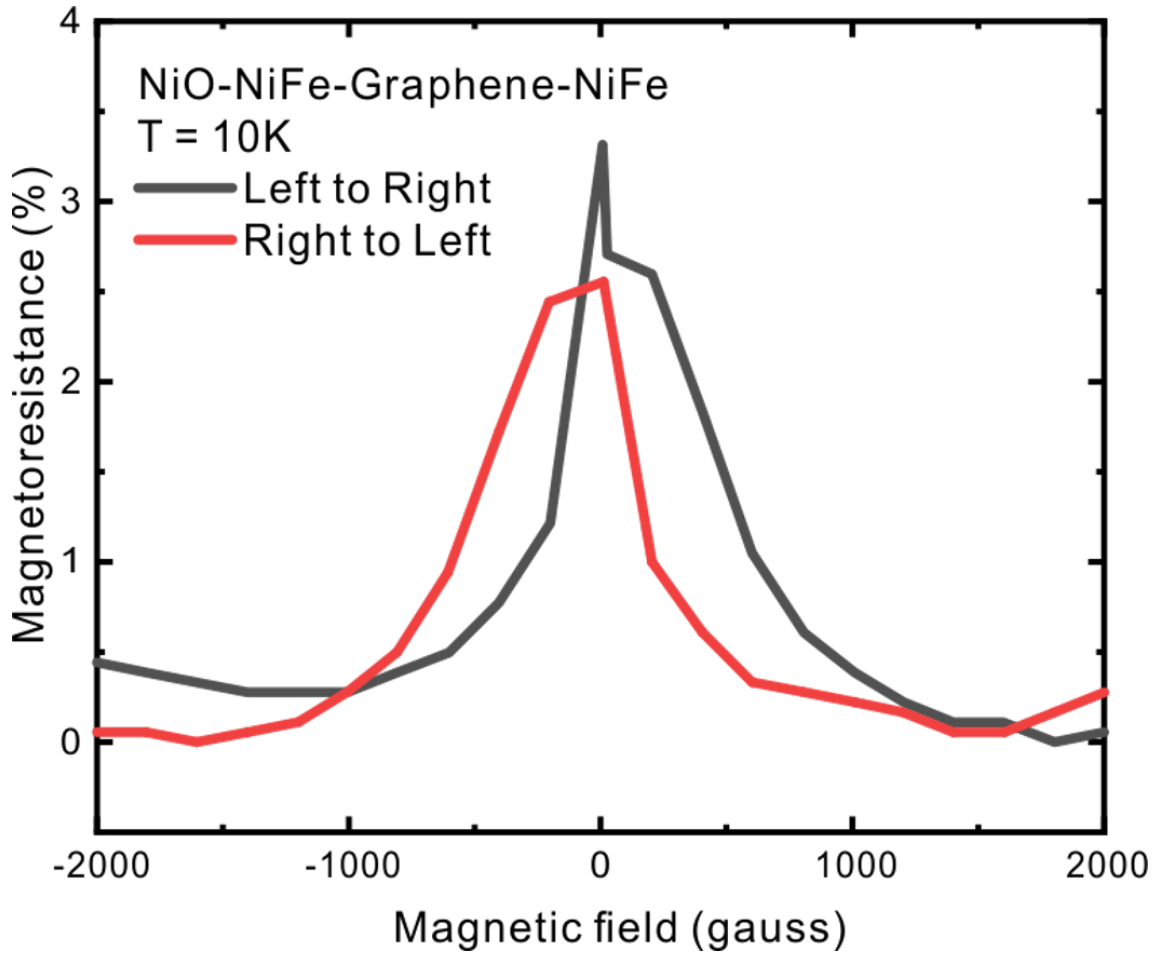

Figure 4.22: Out-plane MR analysis of NiO-NiFe-GSVs.

doi:10.6342/NTU202400068

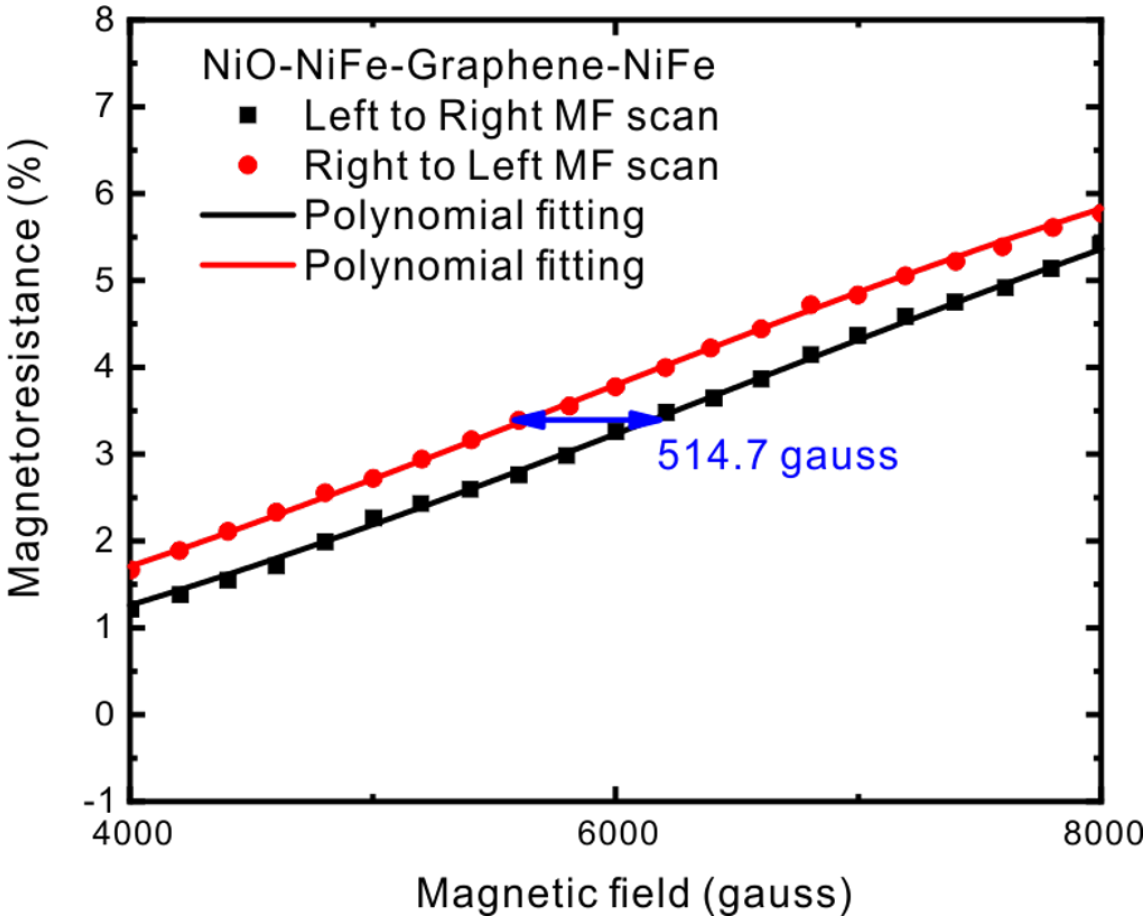

Figure 4.23: Coercivity shift in NiO-NiFe-GSVs.

doi:10.6342/NTU202400068

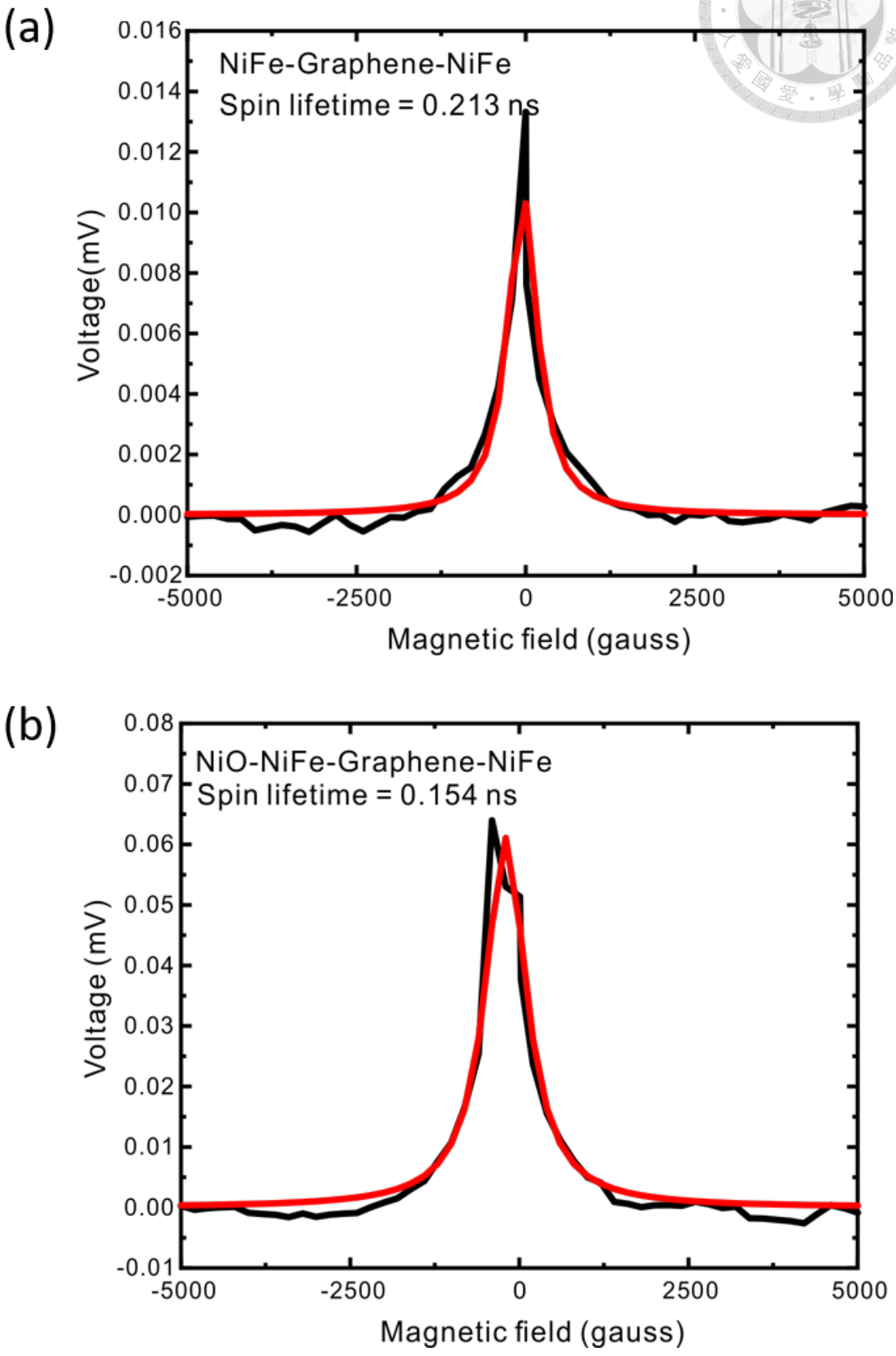

Figure 4.24: Spin lifetime analysis in (a) NiFe-GSVs and (b) NiO-NiFe-GSVs.

doi:10.6342/NTU202400068

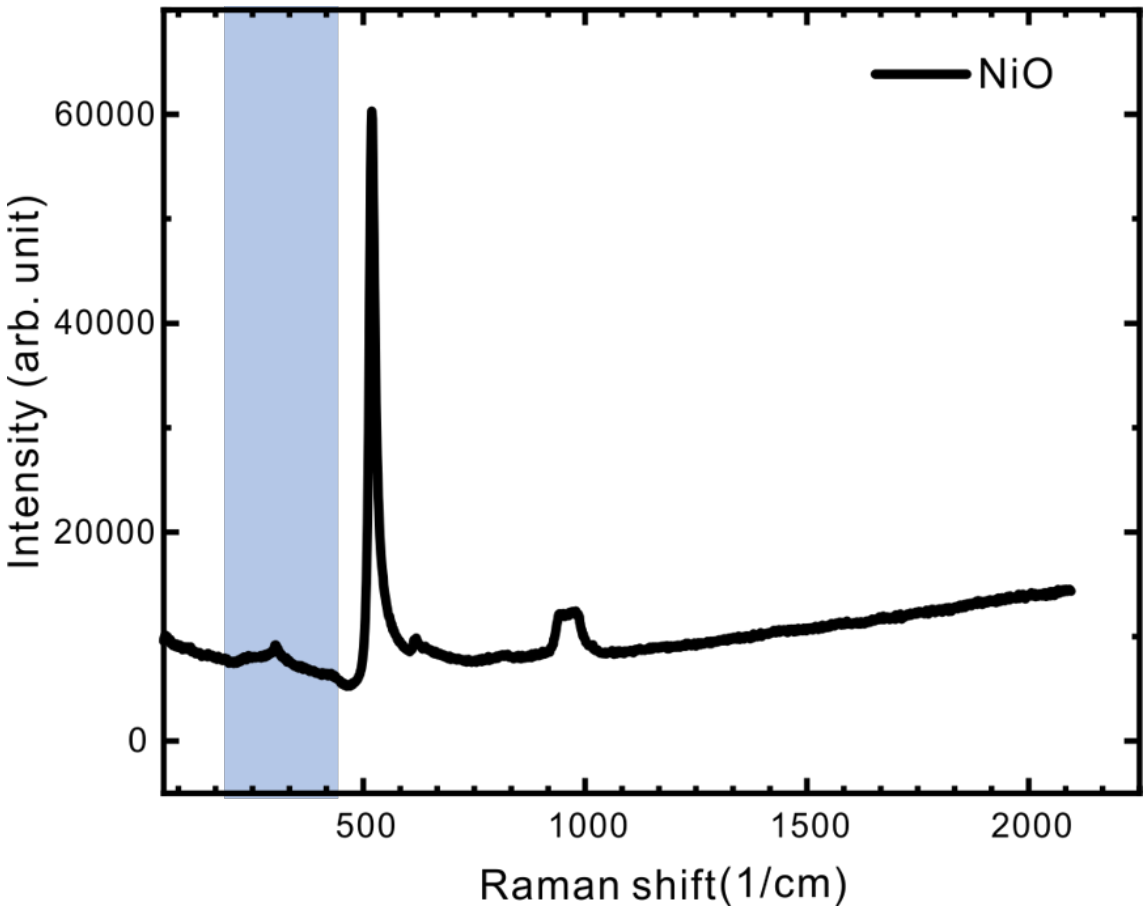

Figure 4.25: Raman spectroscopic result of NiO shows oxygen defects at the feature 310 cm^{-1} highlighted by the blue color.

doi:10.6342/NTU202400068

4.3 Negative MR in MoS_2-based spin valves induced by spin filtering

Exploration of Co/MoS_2/Co spin valves is propelled by distinctive features evident in prior studies. MoS_2, acting as a spacer, induces magnetic anisotropy through charge donation at the Co/MoS_2 heterojunction, offering the potential for tailored spin dynamics.[55] Additionally, MoS_2's semiconducting nature and stable spin polarization make it an intriguing candidate for spin valves.[27, 56, 57] The giant perpendicular magnetic anisotropy and induced metallic behavior of single-layer MoS_2 near Co contribute to understanding spin transport and band hybridization.[58, 59] These characteristics are crucial for advancing spintronics and exploring novel device functionalities. However, MoS_2-based spin valves fall short of theoretical expectations due to inferior interface quality.[60, 61] The UCD method is anticipated to optimize MoS_2-based spin valves and unveil fundamental mechanisms. We constructed Co/multilayer MoS_2/Co structures, named ML-MSVs, using the UCD method, followed by an exploration of their electrical and magnetic properties.

4.3.1 Raman spectroscopic characterization

In our Raman spectroscopy analysis, we distinctly identified two prominent features of MoS_2, namely E_{2g} and A_{1g} modes. The observed shift of 24 cm^{-1} between these two modes is indicative of the multilayer nature of MoS_2. Additionally, our Raman mapping results further validate the presence of multilayer MoS_2, revealing that it is fully suspended within the holes of the substrate. (Figure 4.26)

doi:10.6342/NTU202400068

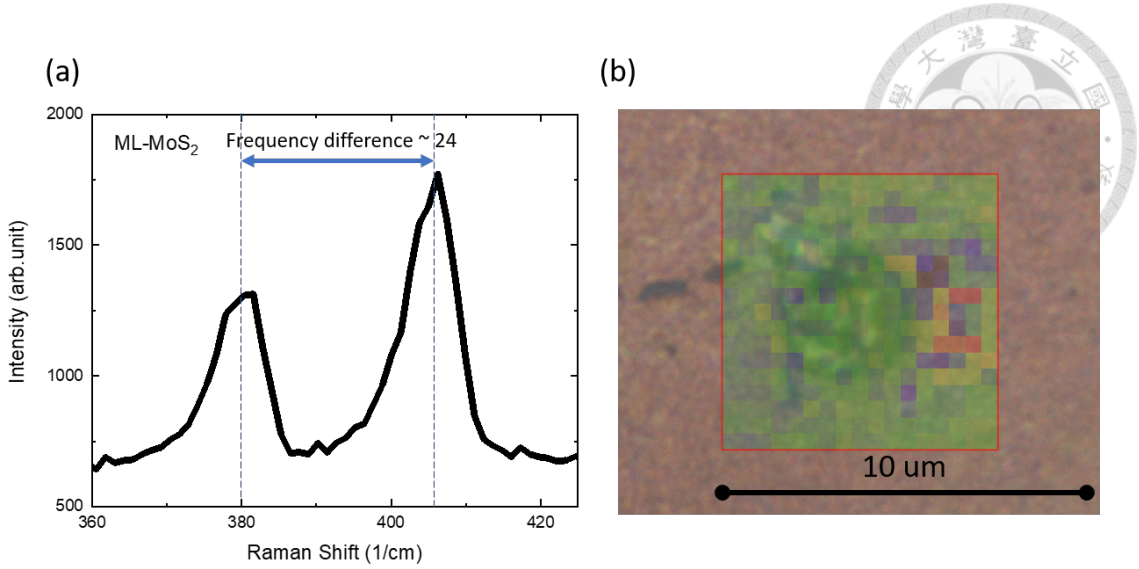

Figure 4.26: (a) Multilayer MoS_2 Raman spectrum, and (b) Raman mapping confirms MoS_2 is suspended on the hole.

4.3.2 Analysis of electric property

The non-linear current-voltage relationship with different temperatures, illustrated by Figure 4.27(a) to (c), signifies prevalent tunneling behavior in electron transport. The asymmetrical curve confirms the efficient separation of both electrodes by the MoS_2 spacer with asymmetric thicknesses. The RT plot (depicted in Figure 4.27(d)) exhibits a distinctive semiconductor curve, underscoring the significant impact of MoS_2 on the electronic properties and supporting its predominant role within the configuration of ML-MSVs.

4.3.3 Magnetotransport in MoS_2-based spin valves

In contrast to graphene-based spin valves (UCD-GSVs or NiFe-GSVs), ML-MSVs exhibit negative MR. The spin filter effect of MoS_2 governs spin transport, resulting in more minority spin carriers tunneling through the barrier in small magnetic fields. Conversely, in large magnetic fields, the majority of spins align in the same direction, permitting only a small quantity of minority spin carriers to pass through the spin filter.

doi:10.6342/NTU202400068

Remarkably, ML-MSVs show a -55% MR at 150K with a bias voltage of -7V under a perpendicular magnetic field (Figure 4.28), surpassing expectations and other comparable studies.[19, 27, 49, 61–64] (see table 4.3) This indicates perpendicular magnetic anisotropy due to metallic proximity between Co and MoS_2. As the temperature increases, negative MR is observed in ML-MSVs. Surprisingly, not only is clear MR observed at room temperature, but the change in MR is enhanced at high temperatures. We infer that MoS_2, exhibiting semiconductor characteristics, displays lower resistance at elevated temperatures, facilitating increased spin carrier flow between electrodes. Conversely, at lower temperatures, the variation in the absolute value of MR is primarily attributed to asymmetry in the quantity of spins aligned in different directions between the two ferromagnetic electrodes (Figure 4.28(d)). However, this aspect still requires further study and discussion.

Structure	MR (%)	Method	Reference
$Fe_3O_4/MoS_2/Fe_3O_4$	0.4	Exfoliation	Wu H-C *et al* (2015)
$NiFe/MoS_2/NiFe$	0.73	Exfoliation	Weiyi Wang *et al* (2015)
$NiFe/MoS_2/Co$	2.0	Exfoliation	Dankert A *et al*(2017)
$NiFe/ML\text{-}MoS_2/Co$	3.0	Exfoliation	Muhammad Farooq Khan *et al* (2018)
$Co/ML\text{-}MoS_2/Co$	-60	UCD	Our work

Table 4.3: MR comparison in MoS_2-based spin valves

In traditional magnetic tunnel junctions, MR tends to decrease with increasing applied bias due to higher voltage leading to increased electron scattering during transmission due to the inelastic scattering given by magnon excitation. However, in our fabricated ML-MSVs, this phenomenon is not observed (see Figure 4.29). To comprehensively explain this discrepancy, additional magnetic measurements, such as VSM (Vibrating Sample Magnetometry) or MOKE (Magneto-Optic Kerr Effect), are needed for further investigation of the underlying mechanisms in this aspect.

In summary, the UCD method optimizes MoS_2-based spin valves, unveiling unique

doi:10.6342/NTU202400068

ML-MSV properties. Unlike graphene-based counterparts, ML-MSVs exhibit negative MR, reaching -55% at 150K, surpassing expectations due to the spin filter effect. The absence of MR decline with bias voltage suggests an interplay between Co and MoS_2 in the electronic structure. This study unveils intriguing behavior in ML-MSVs, marking a significant advancement in spintronics research.

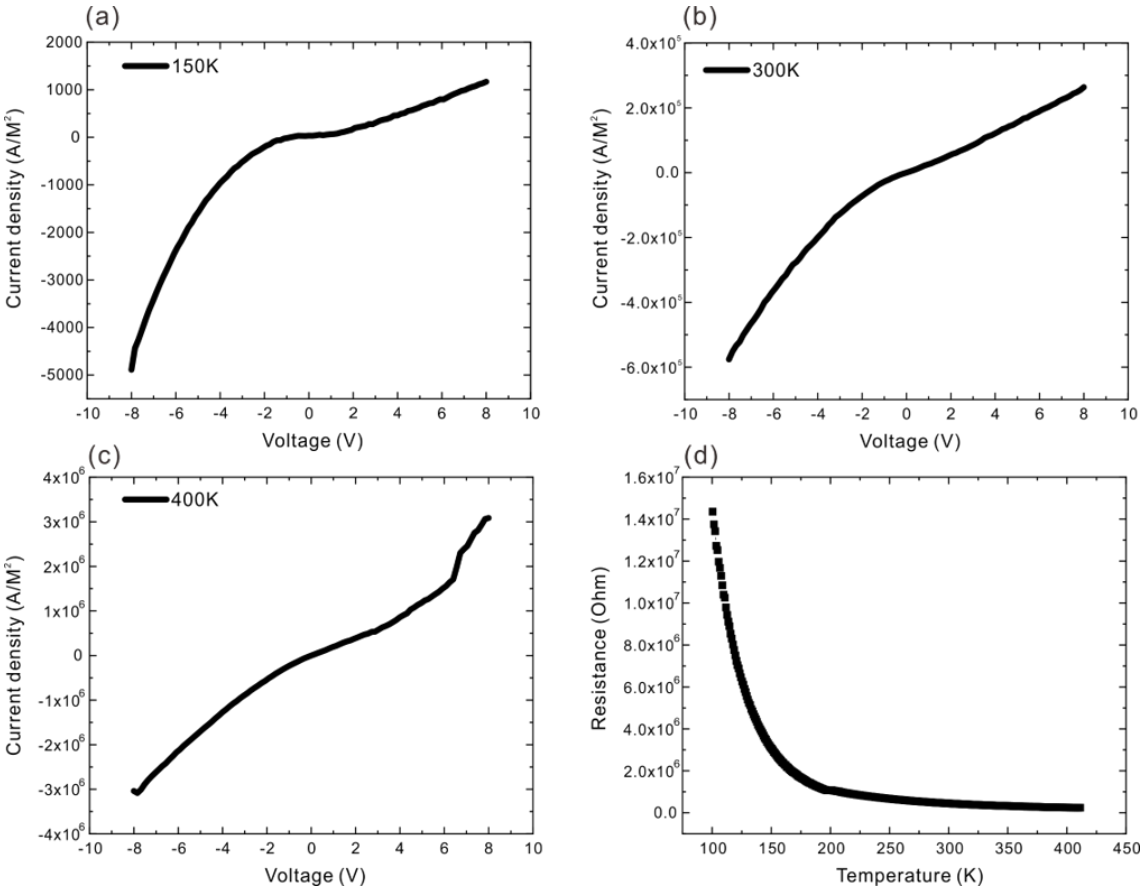

Figure 4.27: (a),(b), and (c) illustrate the temperature-dependent IV curve in ML-MSVs.

doi:10.6342/NTU202400068

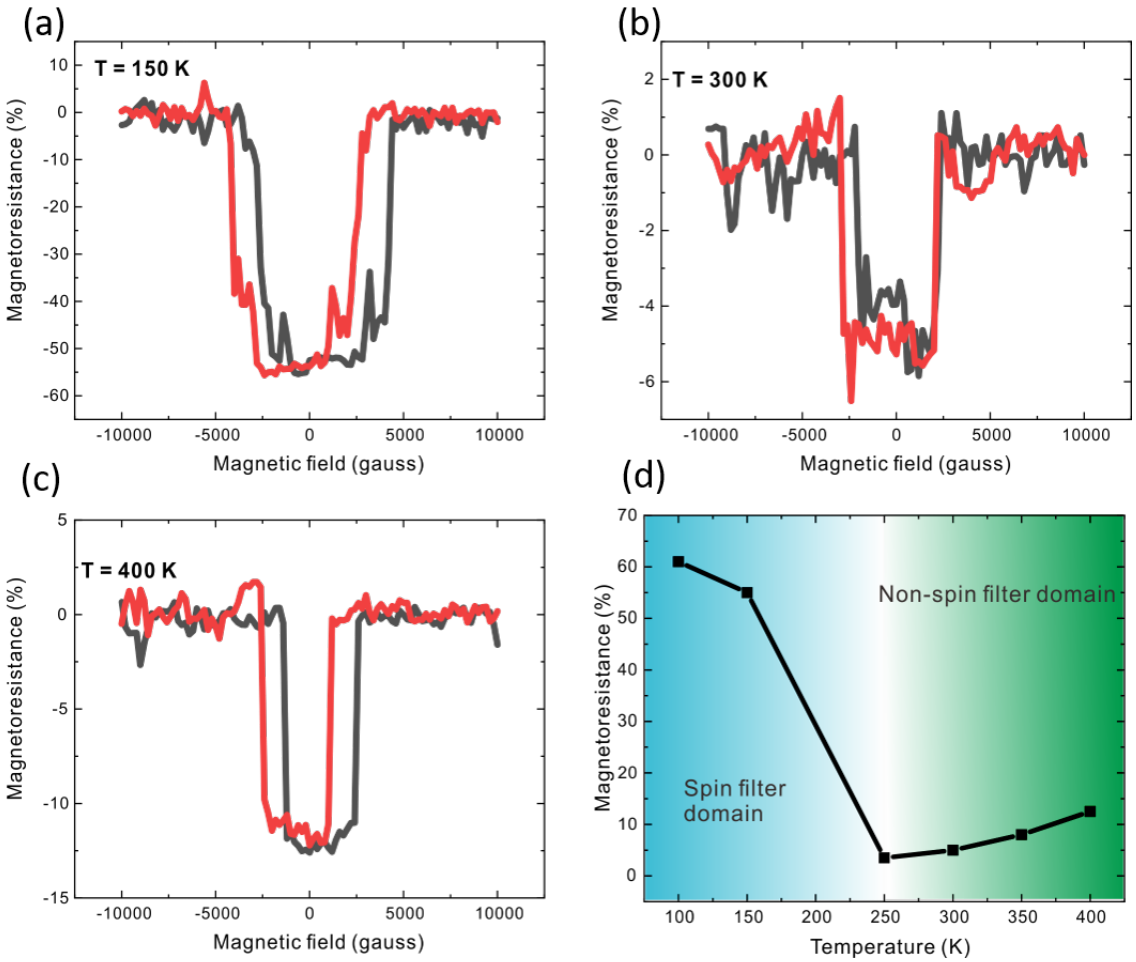

Figure 4.28: (a) to (c) illustrate the temperature-dependent MR in ML-MSVs, and (d) summarizes the MR change as temperature.

doi:10.6342/NTU202400068

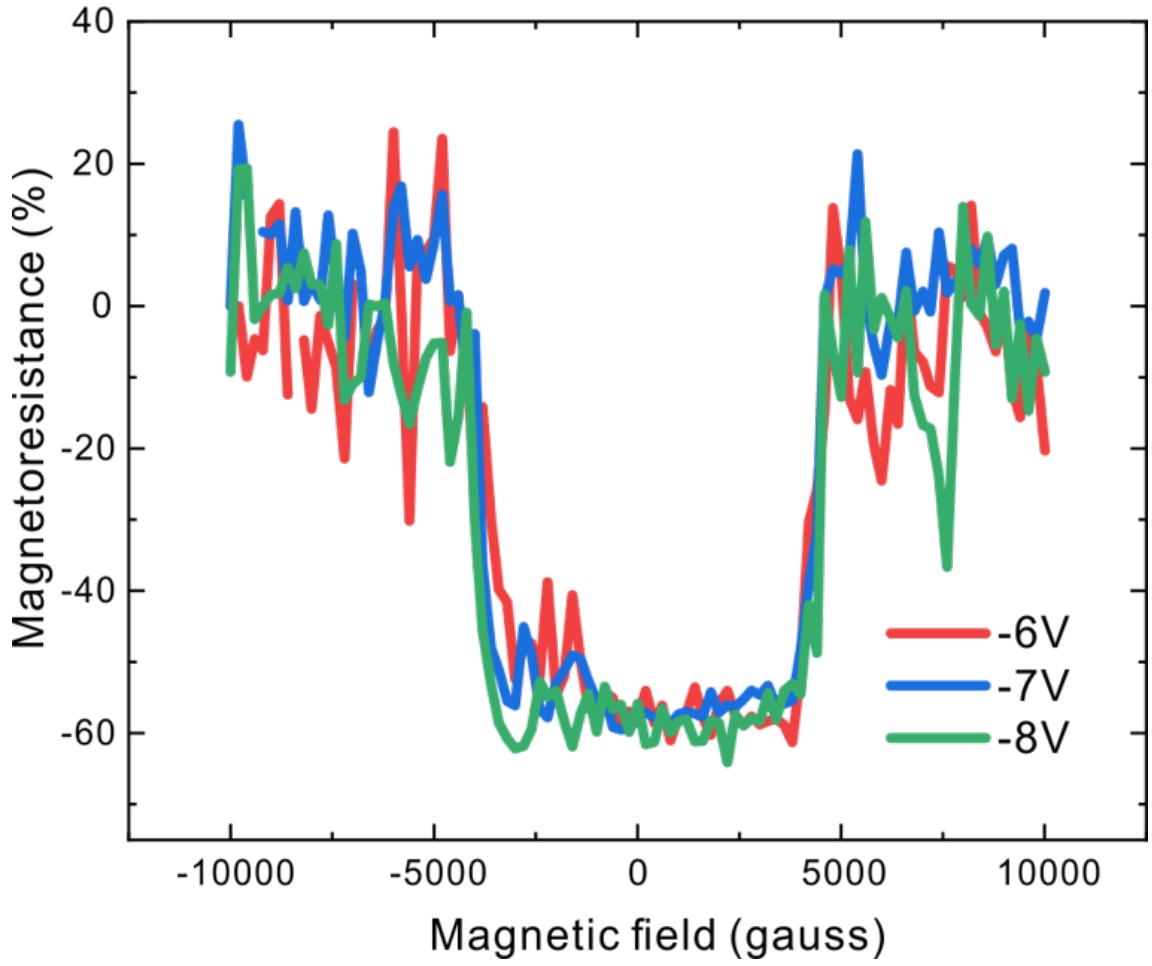

Figure 4.29: Voltage-dependent MR measurement at 100K for ML-MSVs.

doi:10.6342/NTU202400068

Chapter 5 Conclusion

In this study, we aimed to address the specific issues related to spin transport and delve into the associated 2D materials employed in spintronics devices. Our objective was to produce an ultraclean interface in the 2DM spin valve in order to effectively enhance the MR efficiency. Compared to previous studies, all of our MR results exhibit advancements with 1 to 2 orders of magnitude higher efficiency. This underscores the distinctive contribution of the UCD method to the field of spin valve fabrication. The mechanism of spin transfer becomes more readily apparent after eliminating interface contamination. We uncovered that spin scattering is another factor limiting spin transport, a consideration not commonly included in theoretical predictions for UCD-GSVs. In addition to exploring the applications of 2D materials (2DMs), the UCD method proves valuable in showcasing the intrinsic potential of ferromagnetic electrodes. NiFe-GSVs, exhibiting near-zero coercivity characteristics of NiFe, further demonstrate the tunability of coercivity through antiferromagnetic NiO, facilitated by exchange-bias coupling. ML-MSVs exhibit a robust spin-filter effect, as evidenced by the negative MR. Surprisingly, MoS_2 displays two distinct dominant features at different temperature ranges. Our results suggest that ML-MSVs hold promise for application as a potential spintronic device at room temperature. While our study has made important discoveries, there are certain limitations, such as the spin-scattering effect. Future research could further deepen the understanding of the

doi:10.6342/NTU202400068

spin transport mechanism, especially in the areas of unexplored 2DMs application on spin valves. In summary, this study introduces a valuable approach to the fabrication of 2D-material-based spin valves, emphasizing an ultraclean interface and providing a guideline for future research. We anticipate that this research will positively influence both the academic community and practical applications.

doi:10.6342/NTU202400068

References

[1] SA Wolf, DD Awschalom, RA Buhrman, JM Daughton, von S von Molnár, ML Roukes, A Yu Chtchelkanova, and DM Treger. Spintronics: a spin-based electronics vision for the future. science, 294(5546):1488–1495, 2001.

[2] Fabio Pulizzi. Spintronics. Nature materials, 11(5):367–367, 2012.

[3] Igor Žutić, Jaroslav Fabian, and S Das Sarma. Spintronics: Fundamentals and applications. Reviews of modern physics, 76(2):323, 2004.

[4] Bernard Dieny, Ioan Lucian Prejbeanu, Kevin Garello, Pietro Gambardella, Paulo Freitas, Ronald Lehndorff, Wolfgang Raberg, Ursula Ebels, Sergej O Demokritov, Johan Akerman, et al. Opportunities and challenges for spintronics in the microelectronics industry. Nature Electronics, 3(8):446–459, 2020.

[5] Yiming Huai, Frank Albert, Paul Nguyen, Mahendra Pakala, and Thierry Valet. Observation of spin-transfer switching in deep submicron-sized and low-resistance magnetic tunnel junctions. Applied Physics Letters, 84(16):3118–3120, 2004.

[6] Jun-Yang Chen, Yong-Chang Lau, JMD Coey, Mo Li, and Jian-Ping Wang. High performance mgo-barrier magnetic tunnel junctions for flexible and wearable spintronic applications. Scientific reports, 7(1):42001, 2017.

doi:10.6342/NTU202400068

[7] K Ryu. A magnetic tunnel junction based zero standby leakage current retention flip-flo. IEEE Trans. VLSF System, (99):1–10, 2011.

[8] De-Hua Han, Jian-Gang Zhu, and Jack H Judy. Nife/nio bilayers with high exchange coupling and low coercive fields. Journal of applied physics, 81(8):4996–4998, 1997.

[9] L. Wu et al. Atomically sharp interface enabled ultrahigh-speed non-volatile memory devices. Nature Nanotechnology, 16(8):882–887, 2021.

[10] Haikel Sediri, Debora Pierucci, Mahdi Hajlaoui, Hugo Henck, Gilles Patriarche, Yannick J Dappe, Sheng Yuan, Bérangère Toury, Rachid Belkhou, Mathieu G Silly, et al. Atomically sharp interface in an h-bn-epitaxial graphene van der waals heterostructure. Scientific reports, 5(1):16465, 2015.

[11] M. Piquemal-Banci et al. 2d-mtjs: Introducing 2d materials in magnetic tunnel junctions. Journal of Physics D: Applied Physics, 50(20):203002, 2017.

[12] V. Karpan et al. Graphite and graphene as perfect spin filters. Physical Review Letters, 99(17):176602, 2007.

[13] Y. Zhang et al. Experimental observation of the quantum hall effect and berry's phase in graphene. Nature, 438(7065):201–204, 2005.

[14] K. S. Novoselov et al. Two-dimensional gas of massless dirac fermions in graphene. Nature, 438(7065):197–200, 2005.

[15] E. Cobas et al. Graphene as a tunnel barrier: Graphene-based magnetic tunnel junctions. Nano Letters, 12(6):3000–3004, 2012.

doi:10.6342/NTU202400068

[16] Ryuta Yagi, Taiki Hirahara, Ryoya Ebisuoka, Tomoaki Nakasuga, Shingo Tajima, Kenji Watanabe, and Takashi Taniguchi. Low-energy band structure and even-odd layer number effect in ab-stacked multilayer graphene. Scientific Reports, 8(1):13018, 2018.

[17] J. A. Miwa et al. Electronic structure of epitaxial single-layer mos_2. Physical Review Letters, 114(4):046802, 2015.

[18] D. R. Klein et al. Electrical switching of a bistable moiré superconductor. Nature Nanotechnology, 18(4):331–335, 2023.

[19] J. Meng et al. Vertical graphene spin valve with ohmic contacts. Nanoscale, 5(19):8894–8898, 2013.

[20] J.-J. Chen et al. Layer-by-layer assembly of vertically conducting graphene devices. Nature Communications, 4(1):1921, 2013.

[21] A. Krayev et al. Dry transfer of van der waals crystals to noble metal surfaces to enable characterization of buried interfaces. ACS Applied Materials & Interfaces, 11(41):38218–38225, 2019.

[22] K. Jo et al. Direct optoelectronic imaging of 2d semiconductor–3d metal buried interfaces. ACS Nano, 15(3):5618–5630, 2021.

[23] T.M. Mohiuddin et al. Graphene in multilayered cpp spin valves. IEEE Transactions on Magnetics, 44(11):2624–2627, 2008.

[24] J.-H. Park and H.-J. Lee. Out-of-plane magnetoresistance in ferromagnet/graphene/ferromagnet spin-valve junctions. Physical Review B, 89(16):165417, 2014.

doi:10.6342/NTU202400068

[25] P. Asshoff et al. Magnetoresistance of vertical co-graphene-nife junctions controlled by charge transfer and proximity-induced spin splitting in graphene. 2D Materials, 4(3):031004, 2017.

[26] S. Gardelis et al. Spin-valve effects in a semiconductor field-effect transistor: A spintronic device. Physical Review B, 60(11):7764, 1999.

[27] M.F. Khan et al. Layer dependent magnetoresistance of vertical mos 2 magnetic tunnel junctions. Nanoscale, 10(35):16703–16710, 2018.

[28] T. Ikuno et al. Electron transport properties of si nanosheets: Transition from direct tunneling to fowler-nordheim tunneling. Applied Physics Letters, 99(2):023107, 2011.

[29] H. Gu et al. An overview of the magnetoresistance phenomenon in molecular systems. Chemical Society Reviews, 42(13):5907–5943, 2013.

[30] Janice Nickel. Magnetoresistance overview. Hewlett-Packard Laboratories, Technical Publications Department Palo Alto ⋯, 1995.

[31] M.N. Baibich et al. Giant magnetoresistance of (001) fe/(001) cr magnetic superlattices. Physical Review Letters, 61(21):2472, 1988.

[32] S. Dash et al. Silicon spintronics at room temperature. In Spintronics III. SPIE, 2010.

[33] O. Van't Erve et al. Spin transport and hanle effect in silicon nanowires using graphene tunnel barriers. Nature Communications, 6(1):7541, 2015.

[34] O.M. Van't Erve et al. Graphene and monolayer transition-metal dichalcogenides: Properties and devices. Journal of Materials Research, 31(7):845–877, 2016.

doi:10.6342/NTU202400068

[35] W. Han et al. Graphene spintronics. Nature Nanotechnology, 9(10):794–807, 2014.

[36] Y. Ahn et al. Thermal annealing of graphene to remove polymer residues. Materials Express, 6(1):69–76, 2016.

[37] Y. Liu et al. The split-up of g band and 2d band in temperature-dependent raman spectra of suspended graphene. Optics & Laser Technology, 139:106960, 2021.

[38] Q.-Q. Li et al. Raman spectroscopy at the edges of multilayer graphene. Carbon, 85:221–224, 2015.

[39] H. Leamy. Charge collection scanning electron microscopy. Journal of Applied Physics, 53(6):R51–R80, 1982.

[40] J.-W. Ci et al. Modulations for quantum electronic material transports by vacuum annealing methods. In SPIN. World Scientific, 2023.

[41] T.-C. Huang et al. Realizing high-quality interfaces in two-dimensional material spin valves. ACS Materials Letters, 6:94–99, 2023.

[42] M. Moosmann et al. Air–water interface of submerged superhydrophobic surfaces imaged by atomic force microscopy. Beilstein Journal of Nanotechnology, 8(1):1671–1679, 2017.

[43] L. Smardz, U. Köbler, and W. Zinn. Oxidation kinetics of thin and ultrathin cobalt films. Journal of Applied Physics, 71(10):5199–5204, 1992.

[44] M.Z. Iqbal et al. Interlayer quality dependent graphene spin valve. Journal of Magnetism and Magnetic Materials, 422:322–327, 2017.

[45] T. Kuczmik et al. Hanle spin precession in a two-dimensional electron system. Physical Review B, 95(19):195315, 2017.

doi:10.6342/NTU202400068

[46] T. Maassen et al. Contact-induced spin relaxation in hanle spin precession measurements. Physical Review B, 86(23):235408, 2012.

[47] W. Han and R.K. Kawakami. Spin relaxation in single-layer and bilayer graphene. Physical Review Letters, 107(4):047207, 2011.

[48] M. Brzhezinskaya et al. Engineering of numerous moiré superlattices in twisted multilayer graphene for twistronics and straintronics applications. ACS Nano, 15(7):12358–12366, 2021.

[49] P. Kumar, A. Kumar, and D. Kaur. Spin valve effect in sputtered fl-mos2 and ferromagnetic shape memory alloy based magnetic tunnel junction. Ceramics International, 47(4):4587–4594, 2021.

[50] J. Ni et al. Electric control of nife/nio exchange bias through resistive switching under zero magnetic field. Journal of Materials Science: Materials in Electronics, 34(6):552, 2023.

[51] I. Lyapilin, M. Okorokov, and V. Ustinov. Spin effects induced by thermal perturbation in a normal metal/magnetic insulator system. Physical Review B, 91(19):195309, 2015.

[52] G. Yu et al. Interface reaction of nio/nife and its influence on magnetic properties. Applied Physics Letters, 78(12):1706–1708, 2001.

[53] C. Catlow et al. The basic atomic processes of corrosion i. electronic conduction in mno, coo and nio. Philosophical Magazine, 35(1):177–187, 1977.

[54] N.J. Usharani and S. Bhattacharya. Effect of defect states in the optical and magnetic

doi:10.6342/NTU202400068

properties of nanocrystalline nio synthesized in a single step by an aerosol process. Ceramics International, 46(5):5671–5680, 2020.

[55] Q. Xie et al. Giant enhancements of perpendicular magnetic anisotropy and spin-orbit torque by a mos2 layer. Advanced Materials, 31(21):1900776, 2019.

[56] Marta Galbiati. Mos2-based vertical spintronic devices. Graphene2017, 2017.

[57] K. Dolui et al. Efficient spin injection and giant magnetoresistance in fe/mos2/fe junctions. Physical Review B, 90(4):041401, 2014.

[58] C. Jiang et al. Robust half-metallic magnetism in two-dimensional fe/mos2. The Journal of Physical Chemistry C, 122(37):21617–21622, 2018.

[59] C.-I. Lu et al. Spontaneously induced magnetic anisotropy in an ultrathin co/mos2 heterojunction. Nanoscale Horizons, 5(7):1058–1064, 2020.

[60] A. Dankert et al. Tunnel magnetoresistance with atomically thin two-dimensional hexagonal boron nitride barriers. Nano Research, 8:1357–1364, 2015.

[61] M.-B. Martin et al. Protecting nickel with graphene spin-filtering membranes: A single layer is enough. Applied Physics Letters, 107(1), 2015.

[62] M.Z. Iqbal et al. Spin valve effect of nife/graphene/nife junctions. Nano Research, 6:373–380, 2013.

[63] M. Iqbal et al. Interlayer dependent polarity of magnetoresistance in graphene spin valves. Journal of Materials Chemistry C, 3(2):298–302, 2015.

[64] H.-C. Wu et al. Spin-dependent transport properties of fe3o4/mos2/fe3o4 junctions. Scientific Reports, 5(1):15984, 2015.

doi:10.6342/NTU202400068